Bis(ethylenethio)tetrathiafulvalene (BET-TTF) and Related Dissymmetrical Electron Donors: From the Molecule to Functional Molecular Materials and Devices (OFETs)

Concepció Rovira*

Institut de Ciència de Materials de Barcelona (CSIC), Campus Universitari de Bellaterra, 08193 Cerdanyola, Spain

Received April 15, 2004

Contents

1. Introduction 5289
2. Synthesis of Donors 5290
   2.1. Symmetric Donors 5290
      2.1.1. Synthesis of BET-TTF and αDT-TTF 5290
      2.1.2. Synthesis of BES-TTF, αDS-TTF, and BES-TSF 5292
   2.2. Dissymmetric Donors 5292
3. Structural Characteristics of Donors 5293
   3.1. Molecular Structures 5293
      3.1.1. Symmetric Donors 5293
      3.1.2. Dissymmetric Donors 5293
   3.2. Crystal Packing 5294
      3.2.1. Symmetric Donors 5294
      3.2.2. Dissymmetric Donors 5296
4. Redox Properties of Donors 5299
5. Molecular Materials: Charge-Transfer Complexes and Radical–Ion Salts 5299
   5.1. From Symmetric Donors 5299
      5.1.1. BET-TTF Derivatives 5299
      5.1.2. BES-TTF, BES-TSF, and DS-TTF Derivatives 5308
   5.2. From Dissymmetric Donors 5310
      5.2.1. ETT-TTF Derivatives 5310
      5.2.2. ETEDT-TTF Derivatives 5311
6. Conducting Bilayered Films 5313
7. Organic Field-Effect Transistors Based on Single Crystals of Tetrathiafulvalene Derivatives 5314
8. Concluding Remarks 5315
9. Acknowledgments 5315
10. References 5315

Concepció Rovira was born in Vic (Catalunya, Spain) and obtained her Ph.D. degree from the University of Barcelona (Spain) in 1977 working in physical organic chemistry with Manuel Ballester. She was a postdoctoral fellow in 1982/1983 at The Johns Hopkins University with Dwaine O. Cowan working on TTF-based organic metals. She was appointed Colaborador Científico of the CSIC in 1987, and in 1991 she moved to the Institut de Ciència de Materials de Barcelona (CSIC), where was promoted to Full Professor in 2004. She has been a co-author of over 200 journal articles and book chapters and has co-edited two books. Her research interests focus on molecular functional materials and molecular nanoscience and, in particular, in the fields of organic conductors, electron-transfer phenomena, and molecular magnetism.

1. Introduction

In the search for functional molecular materials with a specific physical property, the election of the suitable building block having adequate electronic, functional, and structural characteristics is critical to achieve the appropriate supramolecular organization giving rise to the desired property.

TTF derivatives are versatile building blocks to form supramolecular aggregates in the solid state with interesting conducting and magnetic properties. Those properties are associated with specific interactions between molecules having one or more unpaired electrons, and control of the intermolecular interactions permits modification of the bulk properties of the material. In fact, low-dimensional molecular charge-transfer salts based on TTFs present a wide scope of electronic and magnetic properties ranging, as far as conducting properties are concerned, from semiconductors to metals and superconductors and, in regard to magnetic properties, from Pauli-like paramagnetism and Bonner−Fisher or Heisenberg behaviors to spin Peierls, antiferromagnetic, or canted ferromagnetic ground states.[1] In many cases, there is competition between metallic and insulating, magnetic and superconducting, semiconducting and semimetallic phases.

The reason TTF derivatives have been widely used as building blocks of molecular conductors and magnets lies in their electronic and structural characteristics. Thus, TTFs are good electron donors that form stable open-shell species by transferring one

* To whom correspondence should be addressed. Phone:+34-93-5801853. Fax: +34-93-5805729. E-mail: cun@icmab.es.

10.1021/cr030663+ CCC: $48.50
Published on Web 10/23/2004

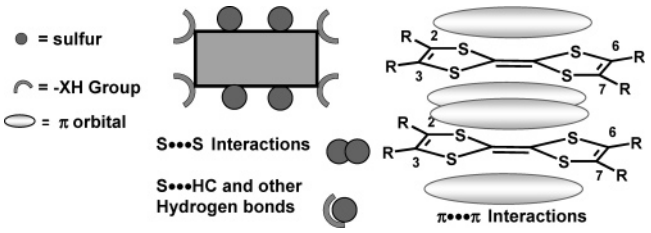

Figure 1. Schematic representation of the supramolecular characteristics of TTF derivatives as well as of the most common interactions in their supramolecular organizations.

π-electron from the HOMO. On the other hand, these molecules have planar shapes that promote their stacking as a consequence of the $\pi-\pi$ orbital overlap. Depending on the packing of the molecules in the solid, the intermolecular electronic interaction, described by the transfer integrals, varies and, as a consequence, the bulk electronic and magnetic properties of the molecular solid can be modified. In addition, it is synthetically possible to introduce a large number of substituents in the 2, 3, 6, and 7 positions of the TTF core,[2] modifying not only the electronic but also the supramolecular characteristics of the TTF derivative (Figure 1).

One of the most successful substituents of the TTF core is the "ethylenedithio" leading to the organic donor BEDT-TTF [bis(ethylenedithio)tetrathiofulvalene] that forms one of the richest families of radical−ion salts, showing an enormous diversity of electronic behavior, including over 70 superconductors.[1c,e] The external sulfur atoms of the BEDT-TTF molecule as well as the ethylene groups play a key role in establishment of the appropriate crystal packing since it has been stated that S···S and C−H···S interactions are very useful as a secondary interactions in order to achieve supramolecular assemblies of TTF derivatives.[3] In addition, it is well known that the S···S interstack overlap promotes a higher electronic dimensionality in a great number of conductors and superconductors.[1] Therefore, a similar TTF building block maintaining such characteristics is a very promising one. We present herein a complete analysis of the electronic and supramolecular characteristics of one donor having these characteristics, bis(ethylenethio)tetrathiofulvalene (BET-TTF). Related donors obtained by substitution of sulfur by selenium atoms are also reviewed as well as the dissymmetrical electron donors containing one ethylenethio substituent. The structural aspects leading to the particular supramolecular organizations in the solid state will be discussed, and their relationship with the specific electronic and magnetic properties of different derived materials will be exposed.

2. Synthesis of Donors

2.1. Symmetric Donors

2.1.1. Synthesis of BET-TTF and αDT-TTF

All known synthesis of BET-TTF donors are based on the phosphite-mediated homocoupling of the corresponding 4,5-dihydrothieno[2,3-*d*]-1,3-dithiole-2-selone, 2-thione, or 2-ketone, one of the most useful methods to prepare TTF derivatives.[2]

The first synthesis of BET-TTF was reported by Engler in 1978 and was achieved by phosphite-mediated coupling of the 4,5-dihydrothieno[2,3-*d*]-1,3-dithiole-2-selone (**4**) prepared following a well-established procedure starting from α-bromo-γ-thiobutirolactone (**1**) (Scheme 1).[4]

Scheme 1

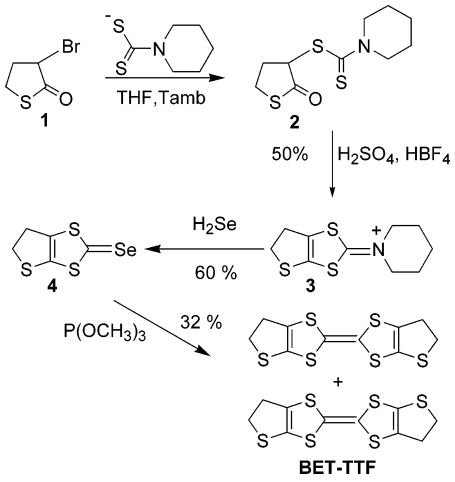

The authors claimed to obtain both isomers of BET-TTF separately based on the different color, solubility, and melting point of two different solids: one that precipitated directly from the reaction mixture and the other obtained by workup of the remaining reaction mixture by chromatography. Nevertheless, any clear evidence of the molecular structure of each was provided.

Thione and ketone analogues of selone **4** were also obtained by the same authors in a very low yield when attempting to prepare the oxygen analogue by cycling the corresponding oxo xantate ester (Scheme 2). Nevertheless, they did not attempt the direct coupling of **6** and **7** to BET-TTF or of **8** to α-DT-TTF (α(thiophene)tetrathiafulvalene).

Scheme 2

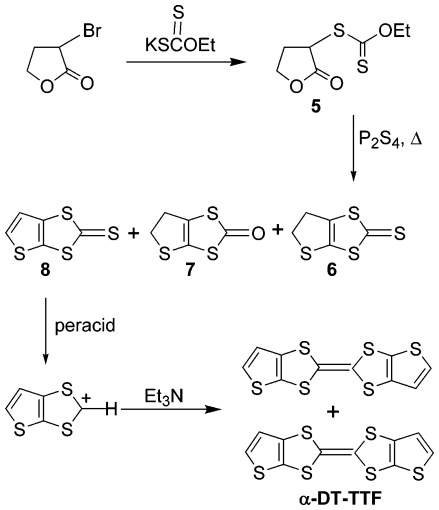

The last donor was however synthesized from thione **8** by treatment with *m*-perchlorobenzoic acid

to give the corresponding dithiolium salt, which was subsequently coupled with triethylamine (Scheme 2).

As in the case of most of the 1,3-dithiole-2-thione derivatives, reaction of thione **6** with mercuric oxide in acetic anhydride provided the corresponding ketone **7**.[4]

Different methodologies to synthesize both thione **6** and ketone **7** have been developed by different authors. The first one involves construction of the 1,3-dithiole-2-thione ring starting with a thiolan-3-one derivative and follows the known route of 1,2,3-thiadiazole thermal decomposition in the presence of carbon disulfide.[5] Thus, treatment of the tosylhydrazone of **9** with thionil chloride effects ring closure to

Scheme 3

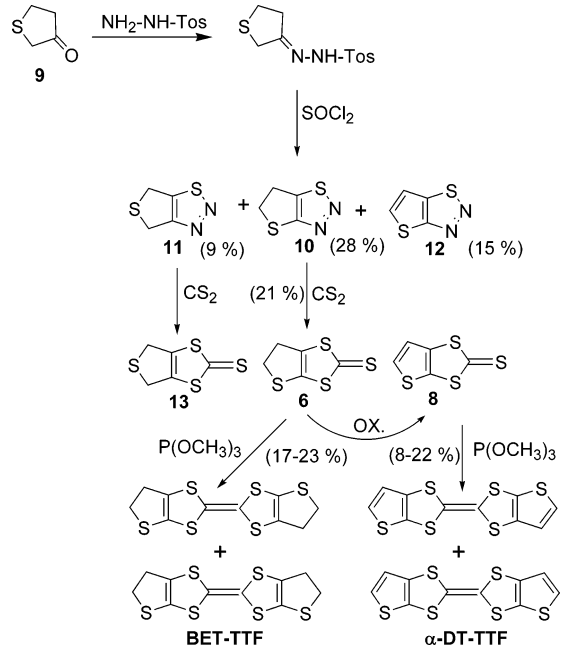

the corresponding 1,2,3-thiadiazoles, cyclization occurring at both α-methylene positions.[6] The aromatic 1,2,3-thiadiazole **12** was also obtained in this reaction. Thermal treatment of **10** and **11** in the presence of carbon disulfide gave the isomeric thiones **6** and **13**. This methodology does not increase the yield in thione **6** obtained by the previous one; the overall

Scheme 4[a]

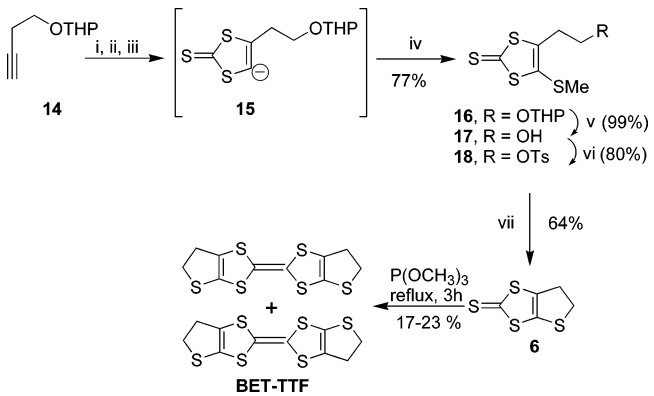

[a] Reagents: (i) n-BuLi, TMEDA, THF; (ii) S; (iii) CS_2; (iv) MeSCN; (v) HCl (aq), acetone/MeOH; (vi) TsCl, pyridine; (vii) NaI, DMF.

yield is around 6%. In contrast, a completely different multistep route, developed by Otsubo et al., which involves construction of the ethylenethio external ring of **6** in the last synthetic step, increased the yield to 40% (Scheme 4). [7]

Ketone **7** can also be obtained directly by an alternative methodology in good yield and gram quantities starting from the α-bromo-γ-thiobutirolactone (**19**) (Scheme 5). [8]

Scheme 5

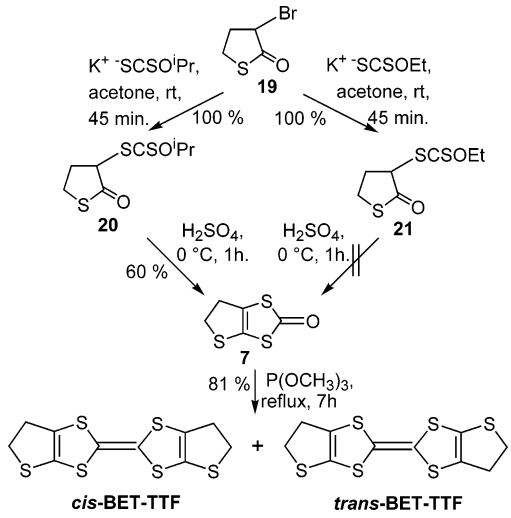

As in the case of the oxygen analogue of thione **6**,[4] all attempts to prepare the oxygen analogue or ketone **7** using the same or similar synthetic procedures failed since the oxo xantate esters obtained cannot be cyclized with acid, yielding instead dimer **23**.[8] The ring closure of **22** was also attempted with P_2O_5, but surprisingly the former oxygen atom of the lactone was replaced by sulfur, giving **7** instead of analogue **24** and therefore leading to a new low-yield procedure for the preparation of **7**.[8] Oxidation of ketone **7** gave the corresponding thiophene analogous in quantitative yield.[9]

Scheme 6

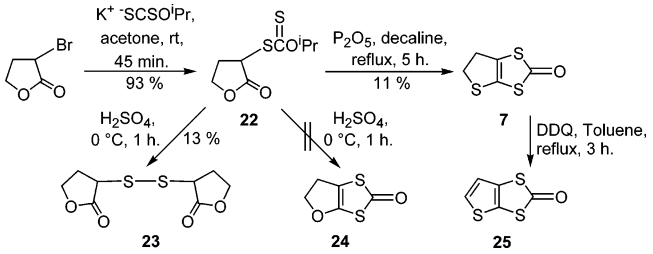

The donor BET-TTF can be obtained by coupling both thione **6** and ketone **7** in refluxing $P(OMe)_3$. Similar to the results with other TTF derivatives having sulfur atoms directly attached to the TTF core,[10,2] coupling of ketone **7** gives a much higher yield (81%)[8] than that of thione **6** (17−23%).[6, 7]

These results point toward the methodology depicted in Scheme 5 as the method of choice for efficient synthesis of gram quantities of the donor BET-TTF.

Also, the corresponding aromatic donor αDT-TTF can be obtained in moderate yields by coupling both thione **8**[6,7a] and ketone **25**[11] in refluxing $P(OMe)_3$.

In all cases the TTF derivatives BET-TTF and αDT-TTF were obtained as a mixture of isomers that shows, in some conditions, distinguishable signals of the methylene protons in the ^1H NMR spectra.[7] By recrystallization of the isomeric mixture of BET-TTF either in CS_2 or chlorobenzene, the isomeric separation of BET-TTF was partially achieved. Thus, the bright red crystals obtained correspond to the *trans*-isomer, although by resolution of the structure (see below) an orientational disorder of between 10% and 15% is always observed;[6] therefore, the presence of a small amount of the *cis*-isomer cannot be ruled out.

2.1.2. Synthesis of BES-TTF, αDS-TTF, and BES-TSF

Different selenium analogues of BET-TTF have been synthesized following the methodology shown in Scheme 4 for the synthesis of BET-TTF. Thus, the TTF derivative bis(ethyleneseleno)tetrathiafulvalene (BES-TTF) was obtained by desulfurization self-coupling of the corresponding thione **29** formed from the vinyl anion **15** (Scheme 7). Thione **29** was easily

Scheme 7[a]

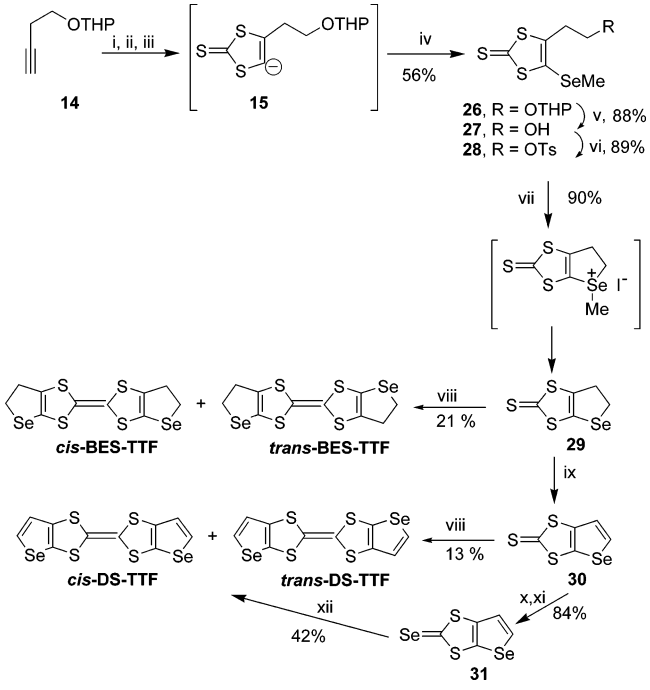

[a] Reagents: (i) n-BuLi, TMEDA, THF; (ii) S; (iii) CS_2; (iv) Se powder, then MeI; (v) HCl (aq), acetone/MeOH; (vi) TsCl, pyridine; (vii) NaI, DMF; (viii) $P(OMe)_3$, reflux; (ix) DDQ, toluene; (x) $(MeO)_2SO_2$, then HBF_4 (aq); (xi) NaHSe, MeOH; (xii) $P(OMe)_3$, benzene, reflux.

converted to the aromatic derivative **30** that by coupling gave αDS-TTF (diselenolotetrathiafulvalene) in poor yield (13%). Nevertheless, this yield was improved to 42% by alternatively using the corresponding selone **31**, which was obtained from **30** by well-established procedures.[7]

Synthesis of the tetraselenafulvalene derivative BES-TSF (bis(ethyleneseleno)tetraselenafulvalene) was achieved by a modified method since the precursor selone **33** is not stable. Instead of creating first the dihydroselenophene ring, the TSF skeleton was achieved from selone **32** and the external rings were later created to give BES-TSF in 39% yield (Scheme 8).

Scheme 8[a]

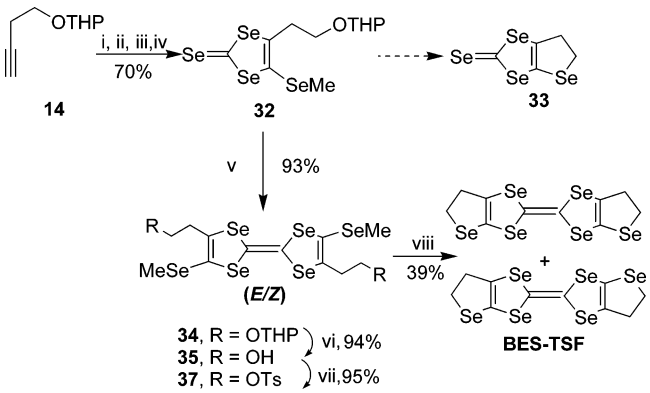

[a] Reagents: (i) n-BuLi, TMEDA, THF; (ii) Se; (iii) CSe_2, Se; (iv) MeI; (v) $P(OMe)_3$, benzene, reflux; (vi) HCl (aq), THF/MeOH; (vii) TsCl, pyridine; (viii) NaI, DMF.

All donors were supposed to be obtained as a mixture of isomers, which was confirmed in the case of BES-TTF and BES-TSF by observation of two signals (1:1 integral ratio) with slightly different chemical shifts for the methylene protons in the ^1H NMR spectra. Nevertheless, as happens in the case of the sulfur analogue αDT-TTF, the isomeric selenophene proton signals of αDS-TTF were indistinguishable.[7]

2.2. Dissymmetric Donors

Several TTF donors having only one ethylenethio substituent have been synthesized. All of them, excluding the simplest one, ethylenethiotetrathiafulvalene (ET-TTF), have been obtained by direct cross-coupling reaction of suitable thiones or ketones in refluxing $P(OMe)_3$ (Scheme 9).[12,13] In most cases

Scheme 9

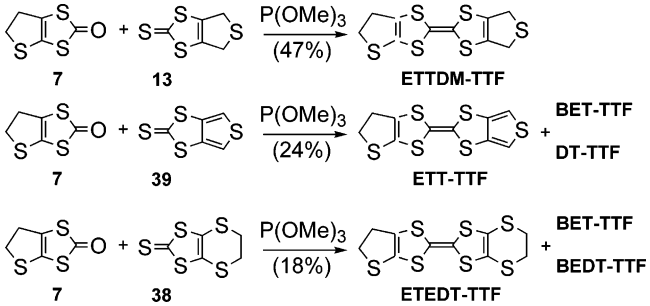

all three possible TTF derivatives were formed in the reaction mixture, and this induced a low yield of the desired dissymmetric compound. The exception is the ETTDM-TTF (ethylenethiothiodimethylene-tetrathiafulvalene) derivative, which was the only donor present in the reaction mixture.[13,14]

Since the yield obtained in the synthesis of ET-TTF through the direct cross-coupling of ketone **7** with 1,3-dithiole-2-thione (**39**) was almost null, an alternative route was used (Scheme 10). Thus, first the dimethoxycarbonyl TTF derivative ETDMC-TTF (ethylenethiodimethoxycarbonyl-tetrathiafulvalene) was synthesized by coupling the suitable ketones with tri-

Scheme 10

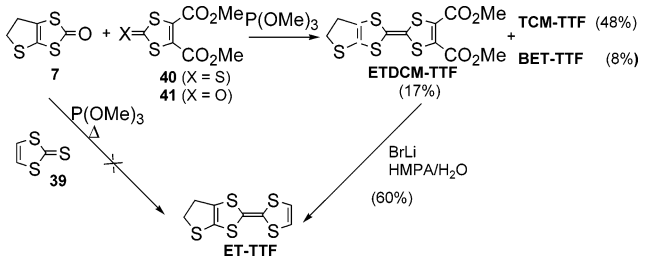

methyl phosphite, and then the resulting donor was decarboxylated to yield the unsubstituted derivative ET-TTF.[12]

3. Structural Characteristics of Donors

3.1. Molecular Structures

3.1.1. Symmetric Donors

BET-TTF can be regarded as being derived from BEDT-TTF by elimination of one of the sulfur atoms of the fused six-membered rings, Chart 1.

Chart 1

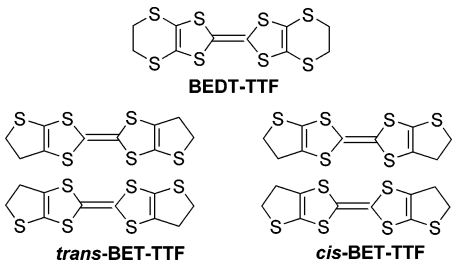

Thus, in BET-TTF the ethylene groups as well as one sulfur atom remain in the same position as in BEDT-TTF. Nevertheless, the five-membered rings in BET-TTF are much more rigid that the six-membered ring of BEDT-TTF, and conformational isomerism due to ethylene groups is not possible. By contrast, BET-TTF has two structural isomers with different symmetry: the cis isomer with C_{2v} symmetry and the trans isomer with C_{2h} symmetry. The selenium analogues BES-TTF and BES-TSF as well as the corresponding aromatic derivatives αDT-TTF and αDS-TTF have the same isomeric characteristics. As observed in other TTF derivatives with the same characteristics,[15] by recrystallization of the mixture of isomers, mainly the trans (C_{2h}) isomer crystallizes. Nevertheless, only in the case of BES-TSF did the crystals analyzed by X-ray diffraction confirm the existence of the pure trans isomer.[7] In fact, the symmetry of both isomers of these molecules facilitates having disordered crystal structures since molecules have two possible ways of packing resulting from a rotation of 180° around the longitudinal axis of the molecule and any of the two possible orientations of the molecules can be inserted in the crystal. This circumstance results in a percentage of orientational disorder of the external chalcogen atoms to be included for the resolution of the crystal structure and cannot be distinguished from the existence of some molecules of the other isomer in the structure.

Molecules of BET-TTF in the crystal structure are almost planar (Figure 2a), whereas those of BES-TSF show a chairlike conformation (Figure 2b) as in other sulfur-substituted TTF derivatives such as BEDT-TTF,[16] BMDT-TTF,[17] and DMET.[18]

3.1.2. Dissymmetric Donors

As in the case of BET-TTF, donors with two different five-membered ring substituents, ETTDM-TTF and ETT-TTF, are almost planar (Figure 3a,b). As can be seen in Figure 3b, the ETT-TTF molecule deviates slightly from planarity since whereas the thiophene ring is nearly planar, the nonaromatic substituent forms an angle of 10.28° or 7.75° (50% disorder) with respect to the molecular mean plane due to folding of the ethylene group. Nevertheless, the disorder present in the molecule prevents having a real view of this point.

By contrast, the ETEDT-TTF molecule deviates significantly from planarity (Figure 3c) due to the six-membered ring boat conformation, as in the case of the symmetric derivative BEDT-TTF.[3,19] On the other hand, the five-membered ring substituent is almost planar, as also occurs in the ETDMC-TTF derivative (Figure 3d) and the symmetric derivative BET-TTF. In contrast, the ethylene group of the ET-TTF molecule is folded with the S5−C9−C8 part forming a dihedral angle of 144° with the TTF plane (Figure 3e). The cause of the great distortion from planarity observed for C9 in the ET-TTF molecule can be found in the especially short C−H···S contacts (2.856 Å)

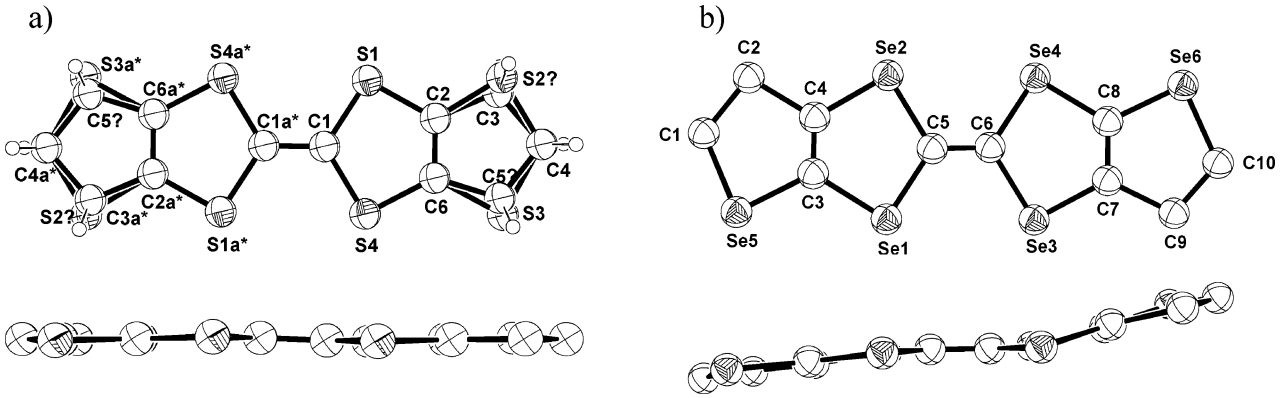

Figure 2. ORTEP representation of the molecular structure of (a) BET-TTF in a perpendicular and parallel view to the plane of the TTF core and (b) BES-TSF in a perpendicular and parallel view to the plane of the TSF core.

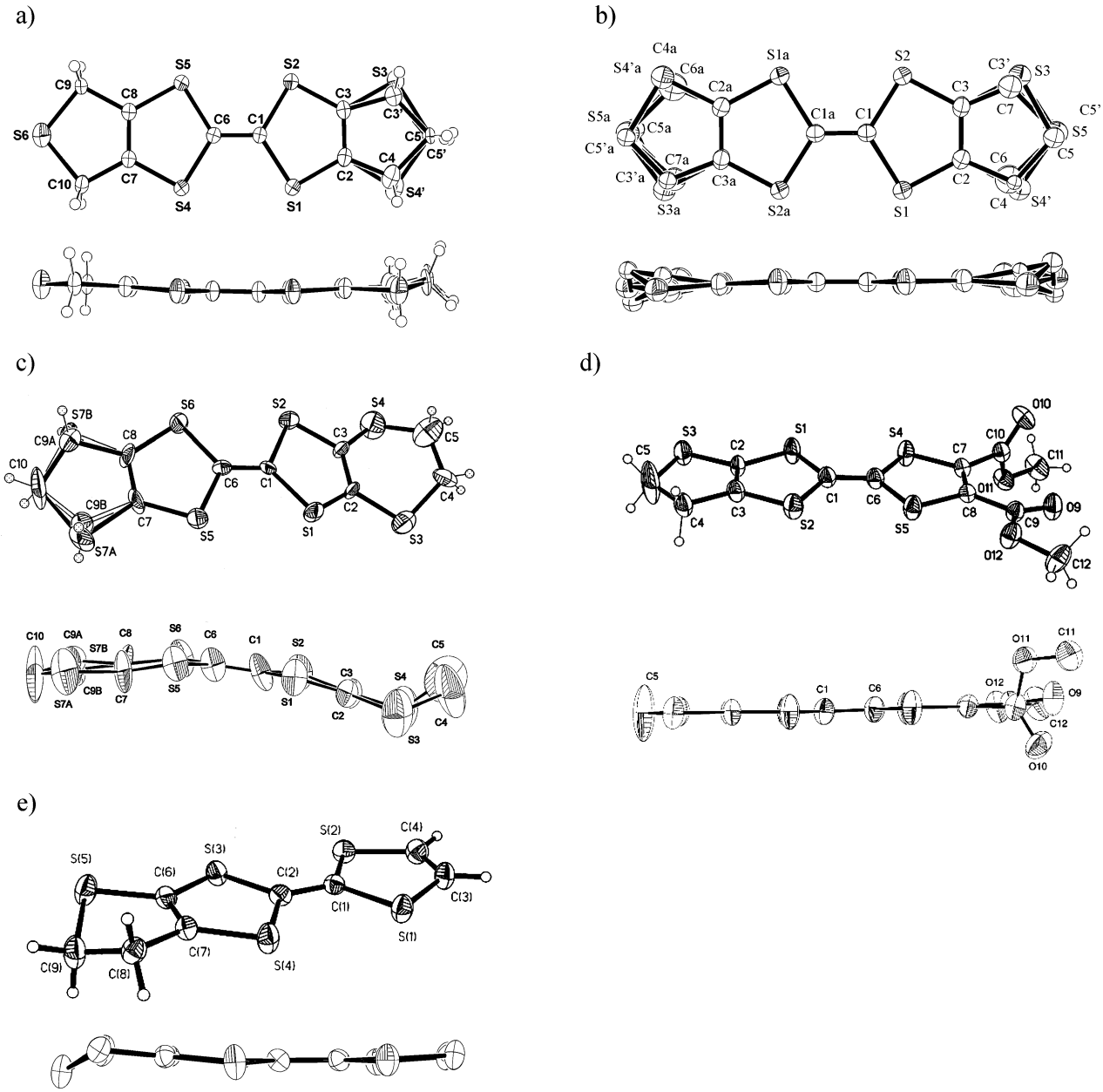

Figure 3. Views of the molecular structure perpendicular and parallel to the plane of the TTF core of (a) ETTDM-TTF, (b) ETT-TTF, (c) ETEDT-TTF, (d) ETDMC-TTF, and (e) ET-TTF.

that are established between C9−H of the molecules in the crystal packing (see below). These hydrogen bonds as well as those formed for the carboxylate groups of the ETDMC-TTF molecule also prevent the disorder in the crystal structures of both donors that is observed in all other dissymmetric donors studied. Thus, ETTDM-TTFs have a disorder of the ethylenethio groups (20%) similar to that observed in the crystal structure of BET-TTF (15%), and in ETEDT-TTF the disorder of the ethylenethio groups is 41−59%. So far the most disordered structure is that of ETT-TTF since there is a 50% disorder in the position of the TTF substituents along the long axis of the molecule; that is 50% of the times is the aromatic ring is in one position and 50% in the dihydrothiophene ring. In addition, there is positional disorder in the sulfur atom of the dihydrothiophene ring being statistically distributed over the two available positions (occupancy factor of 0.5). The disorder observed in all molecules does not affect to the TTF core, and in all these dissymmetric molecules, in contrast to the BET-TTF donor, the disorder is not due to cis−trans isomerization.

3.2. Crystal Packing

3.2.1. Symmetric Donors

The main driving forces behind the packing of molecular crystals are the intermolecular interactions between the molecules that constitute the crystal. It has been found that in neutral TTF derivatives such interactions are the moderately attractive S···S and C−H···S interactions in the −0.35 to −0.60 kcal/mol range.[3] Computation of the molecular electrostatic map (MEP) of a molecule permits one to have an idea of how the hydrogen-bond interactions work collectively, therefore making it possible from these maps to identify the preferred relative orientation of

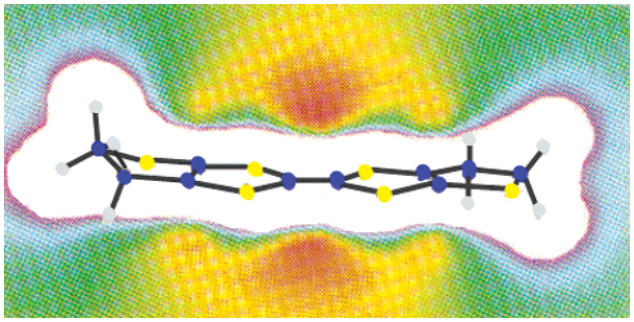

Figure 4. Molecular electrostatic potential map of BET-TTF. In blue are the positive and in red the negative potential areas.

the molecules for the formation of hydrogen bonds. In Figure 4 the MEP map of the trans isomer of BET-TTF is shown in which a plane of symmetry along all the heavy atoms is observed. This map is characterized by two symmetric electron-donating areas located at the end of the molecule on the C−H bonds, and an electron-acceptor area on the rest of the molecule which is stronger on the S atoms. Therefore, the molecule can act as a donor at each end, forming two hydrogen bonds, one above and one below its plane of symmetry, against other molecules.

In accordance with the MEP, the crystal structure of BET-TTF is characterized by a molecule located in the geometrical center of a square connected to four molecules located at the corners by C−H···S bonds in the *c* direction and in the *ab* plane (Figure 5a). These C−H···S bond are reinforced by S···S contacts between the same molecules, and each of these molecules form strong lateral S···S bonds (3.46 Å< d(S···S) < 3.56 Å) along *a,* giving rise to chains of molecules (Figure 5b). Thus, the crystal packing of BET-TTF can be described as being built up from a series of chains of almost planar *trans*-BET-TTF (85% majority orientation) along the *a* direction. These chains stack into layers (Figure 5c) in such a way that the molecules in one chain are displaced along the direction of the long molecular axis with respect to those in adjacent chains. The molecules of every step (i.e., chain along *a*) are also somewhat displaced along *a* with respect to those in adjacent steps (Figure 5d) with an interplanar distance of 3.618 Å.

An accurate analysis of the energy of the S···S interactions of the BET-TTF and of the electronic coupling promoted by these interactions lead to the conclusion that the most important ones are those between the sulfur atoms in the TTF core.[20] This result is due to the fact that, as in the case of BEDT-TTF,[21] the outer sulfur contribution to the HOMO of BET-TTF is considerably smaller (∼1/3) than those of the inner core sulfur atoms. Thus, the effect of the disorder is very small on a whole in the overlap integrals and intermolecular energies.

Crystal packing of BES-TSF[22] is completely different than that observed in BET-TTF. Thus, nonplanar molecules of BES-TSF did not form planar chains; instead, they are packed in the crystal forming zigzag chains along the *b* axis (Figure 6) that are sustained by three Se···Se (3.742, 3.753, 3.732 Å) contacts between perpendicular molecules. These chains are connected along the *c* axis by short Se···Se contacts (3.620 Å) (Figure 6a), forming a two-dimensional arrangement of molecules in layers. In addition, these

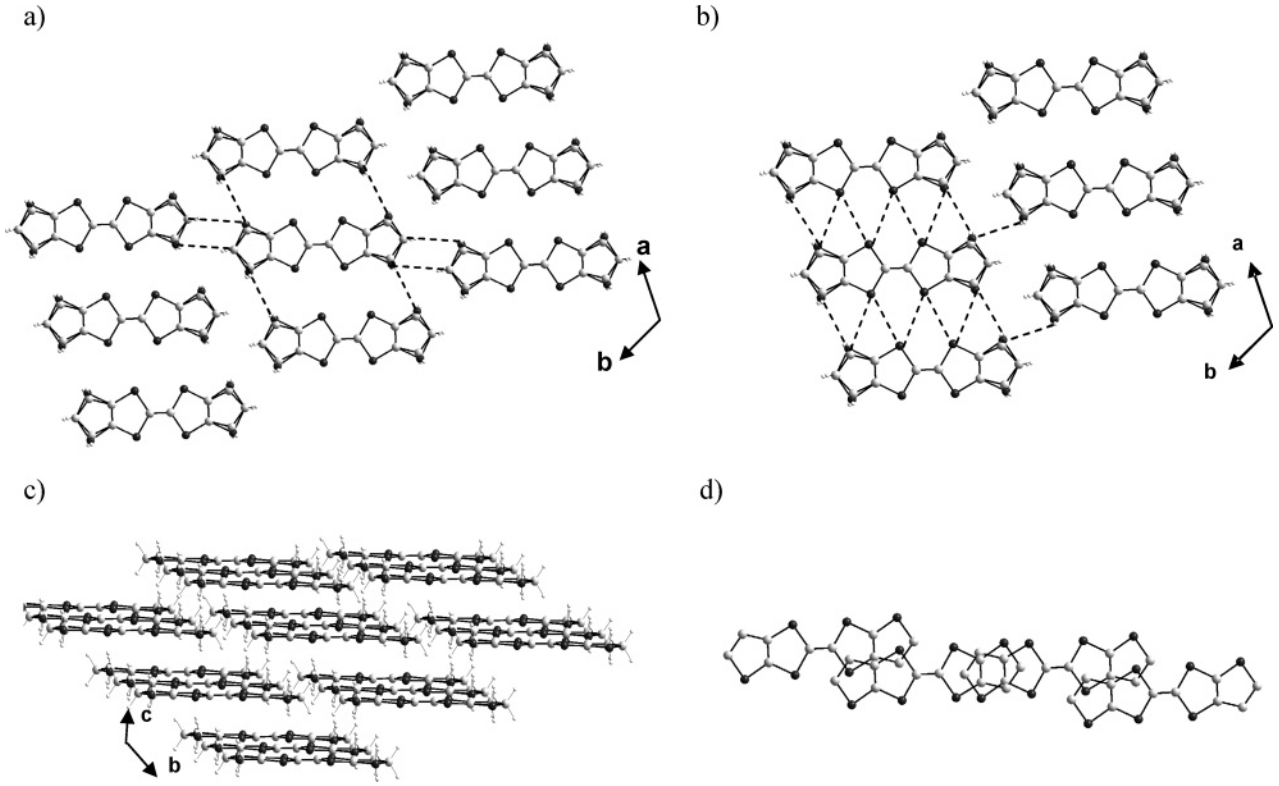

Figure 5. Crystal structure of BET-TTF. (a) Projection view approximately along the direction perpendicular to the BET-TTF molecular plane showing all the C−H···S contacts of one molecule in the *ab* plane. (b) The same projection showing the S···S contacts between molecules. (c) Projection showing the packing of sheets. (d) Overlap modes of molecules.

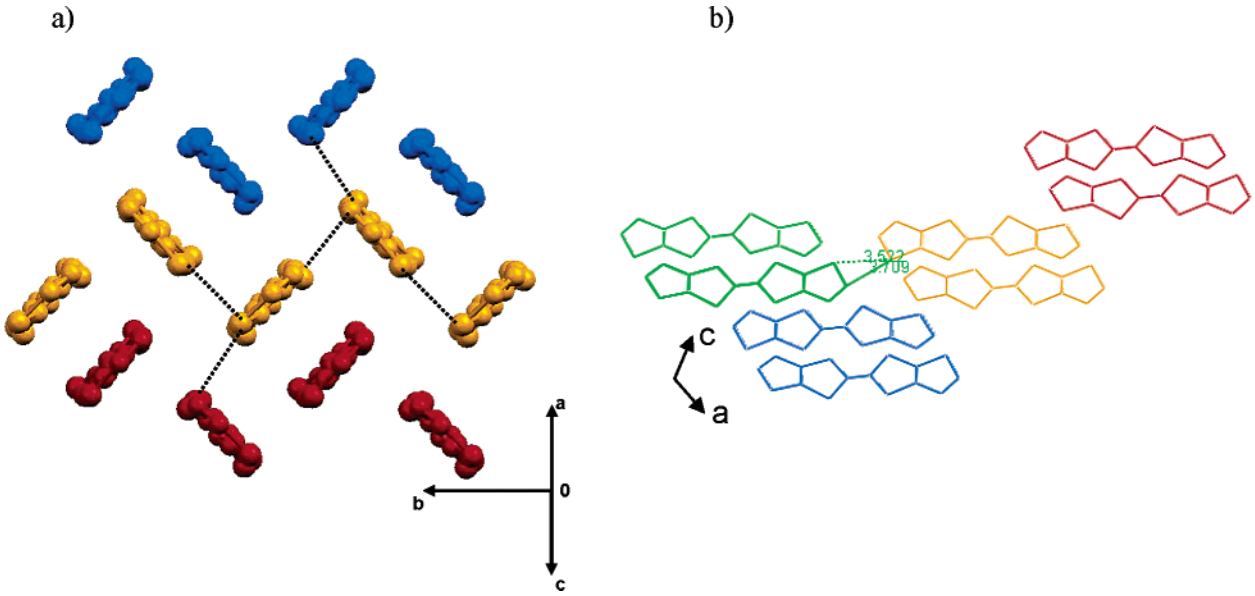

Figure 6. Crystal packing of BES-TSF: (a) view parallel to the longest axis of the molecule showing the zigzag chains and the short Se···Se contacts and (b) view along the *b* axis.

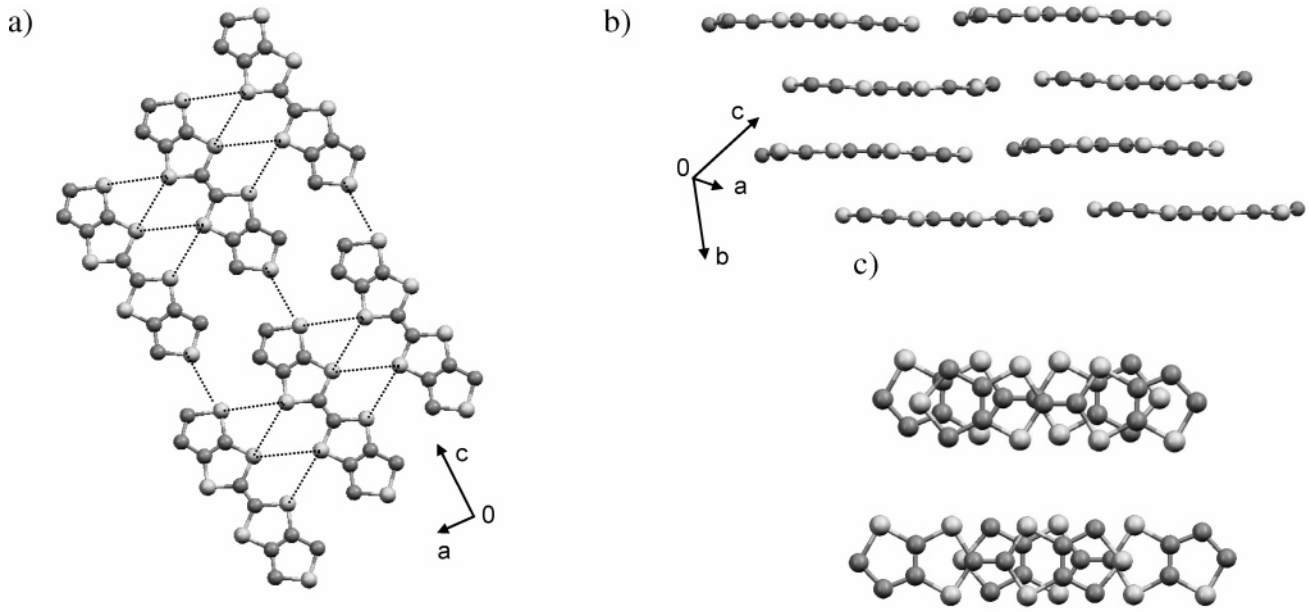

Figure 7. Crystal structure of the dissymmetric ETTDM-TTF donor in which the disorder and the hydrogen atoms have been omitted for clarity: (a) view along the stacking axis *b* (S···S contacts in the *ac* plane as dotted lines), (b) perpendicular view to the stacking axis *b*, and (c) views of intradimer (up) and interdimer overlap (down).

layers are connected in the *ac* plain by one very short Se5···Se5 contact and one C1−H···Se5 bond. Molecules in different chains did not have any kind of $\pi-\pi$ overlap since the distances between planes are too large.

3.2.2. Dissymmetric Donors

The crystal packing of ETTDM-TTF[13,14] is similar to that of BET-TTF and can also be described as being built up from series of chains of quasi-planar molecules along *a* interacting side-by-side by short S···S contacts (Figure 7a). These chains stack into layers (Figure 7b) in such a way that the molecules in one chain are shifted along the direction of the long molecular axis with respect to those in adjacent chains. BET-TTF and ETTDM-TTF structures differ due to the fact that molecules of BET-TTF in one chain are shifted along the direction of the short molecular axis with respect to those in adjacent chains, whereas in ETTDM-TTF this displacement is insignificant, which results in a better interplanar molecular overlap (Figure 7c). Besides, in ETTDM-TTF the stacked chains show formation of dimers along *b*, being the interplanar distance between molecules in the same layer, 3.568 and 3.663 Å for the intradimer and interdimer distances, respectively. As in BET-TTF, many short C−H···S bonds (< 3.20 Å) are also found in the crystal structure of ETTDM-TTF, which is very important in determination of the intralayer and interlayer crystal packing.[23]

The crystal packing of the other donor, with two five-membered rings as substituents, ETT-TTF is completely different.[13,24] Thus, ETT-TTF crystallizes

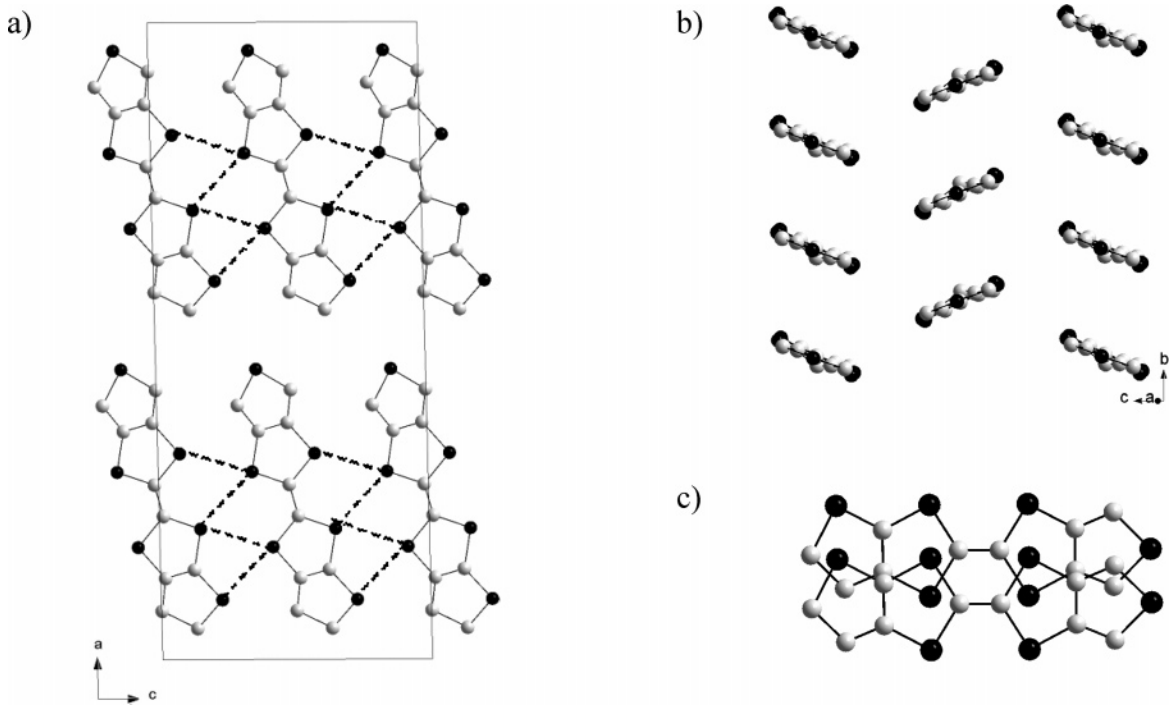

Figure 8. Projection of the crystal structure of ETT-TTF. For clarity purposes, only one of the possible molecules has been drawn. (a) View along the stacking axis *b*; dashed lines show S···S contacts shorter than 4 Å. (b) View parallel to the long molecular axes. (c) Overlap of two consecutive molecules within a stack.

forming uniform stacks of almost planar molecules along the *b* axis in a herringbone pattern, that is adjacent stacks form opposite angles with respect to the stacking axis (Figure 8). The packing of ETT-TTF is almost identical to that of the related symmetric donor DT-TTF (dithiophene-tetrathiafulvalene).[6] The interplanar distance between the molecules along one stack is very short in these crystals (3.66 Å), exhibiting an effective intrastack molecular overlap similar to that found in many conducting salts derived from TTF compounds,[1] particularly in the so-called "α- and *θ*-phases" (Figure 8c). Short intermolecular S···S contacts (3.63 and 3.72 Å) are found between molecules of different stacks along *c* since the sulfur atoms of the external dihydrothiophene ring are also involved in these contacts (Figure 8a).

ETEDT-TTF molecules are packed forming head-to-tail dimers (Figure 9) sustained by C−H···S and C−H···C hydrogen bonds,[12] as happens in BEDT-TTF,[3,16] and other related dissymmetric donors containing the ethylenedithio substituent such as dimethylethylenedithiodizelenadithiafulvalene (DMET-TTF)[25] and ethylenedithiotetrathiafulvalene (EDT-TTF).[26] This is the reason the ETEDT-TTF molecules are not planar, maximizing the energy of the packing by forming these dimers. The dimers are connected through short S···S contacts, forming chains along the *a* direction, and the chains are arranged perpendicularly to each other, avoiding overlap of the dimers to form stacks. The main difference between the BEDT-TTF and ETEDT-TTF crystal structures is the disorder of the ethylenethio groups (59−41%) in ETEDT-TTF.

The packing of the ET-TTF donor shows a similar angular pattern to that of TTF, both compounds forming chains of molecules that are arranged in stacks. In contrast to TTF, which forms linear chains along the *c* direction and overlap along the *a* direction,[27,28] ET-TTF forms zigzag chains along the *ac* direction (Figure 10a) that stacks along the *b* axis in such a way that the molecules form head-to-tail dimers but not stacks of molecules. The stacks of chains have two different orientations with an angle of approximately 60° (Figure 10b). There are short S···S contacts along the chains, between parallel chains, and between nonparallel chains. There are also C−H···S and C−H···C bonds between parallel chains and between chains with different orientation forming a 3-D structure. Especially short C−H···S contacts (2.856 Å) are established between C9−H of a molecules in one chain and S2 of molecules in the next chains with different orientation. These packing characteristics could be the cause of the great distortion from planarity observed for C9 in the ET-TTF molecule.

Finally, ETDCM-TTF has a very different crystal packing than the other derivatives described here, clearly dominated by the hydrogen bonds formed by the methoxycarbonyl groups.[12] ETDCM-TTF forms stacks of molecules along the *a* axis, which are arranged head-to-tail both along the *a* and *b*−*c* directions (Figure 11). There are hydrogen bonds along the stacks, along the *b*−*c* direction, and in the *ab* direction, forming a 3D network. There are also short intrastack and between adjacent stacks S···S contacts.

At this point it is interesting to analyze which part of the molecule controls the packing pattern in the crystals of these dissymmetric donors. In the case of ETDCM-TTF, as expected, the strong hydrogen bonds arising from the carbonyl groups dominate the crystal packing. In the other donors, in which only S···S and C−H····S contacts are responsible for the packing, it was not as straightforward to predict the crystal

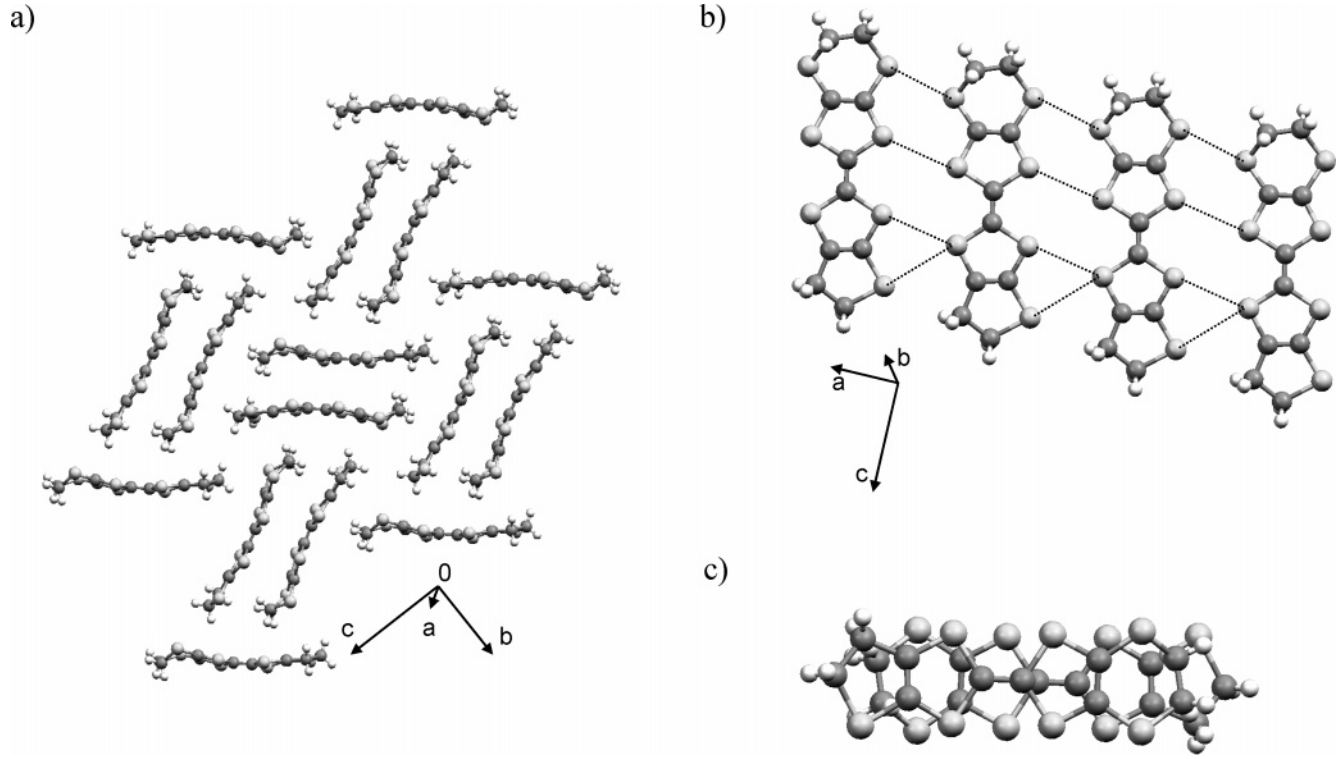

Figure 9. Crystal structure of the dissymmetric ETEDT-TTF donor: (a) view perpendicular to the TTF-core plane, (b) chains along the *a* axis through S···S contacts (dotted lines), and (c) overlap within the dimerized molecules.

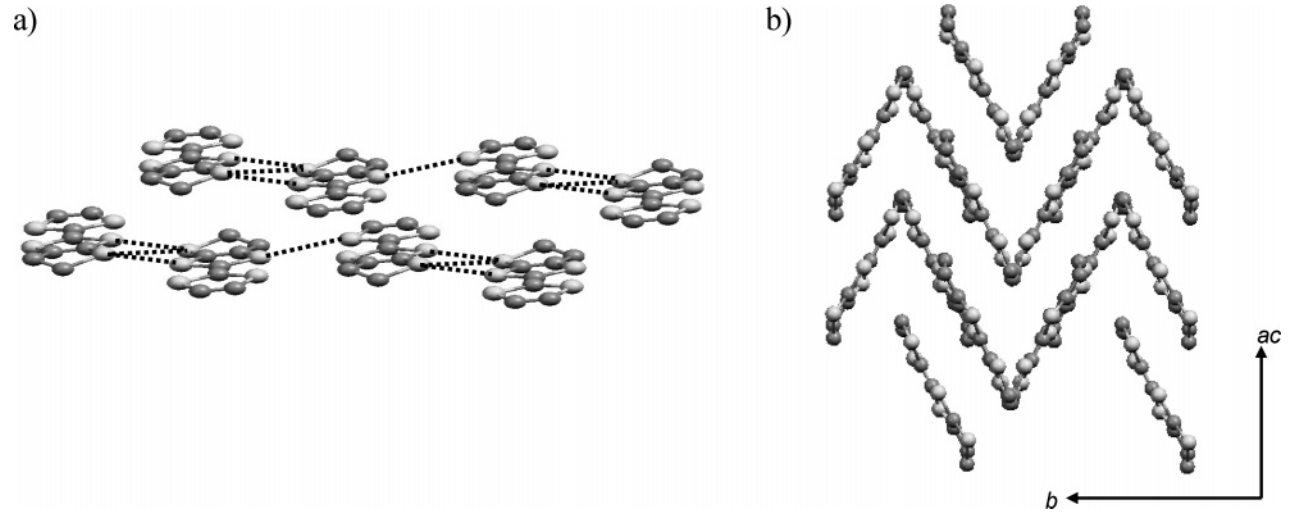

Figure 10. Crystal packing of ET-TTF: (a) view of the chains formed in the *ac* direction showing the short S···S contacts and (b) view of the angular packing.

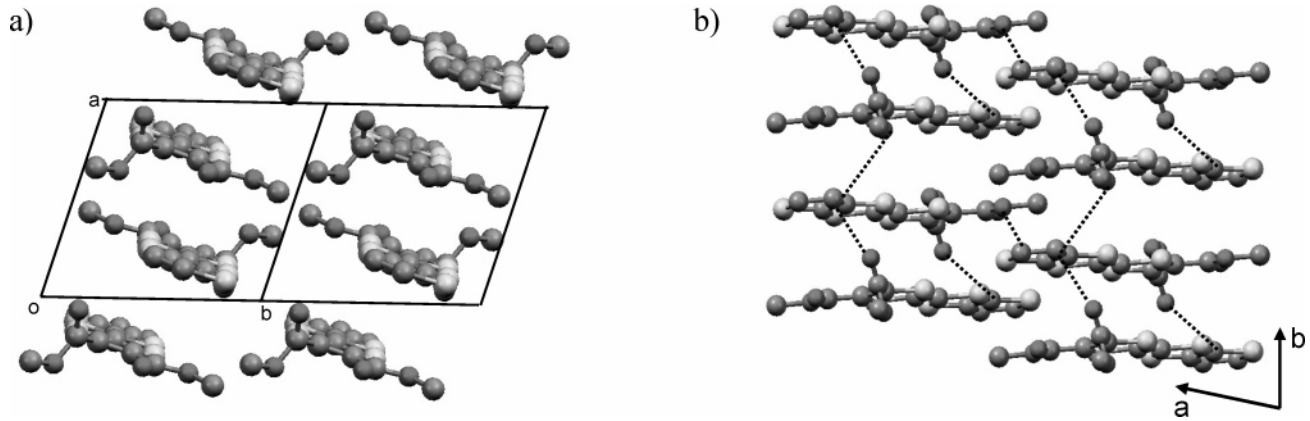

Figure 11. Crystal packing of ETDCM-TTF; hydrogen atoms have been omitted for clarity. (a) Projection perpendicular to the *ac* plane. (b) View along the *c* axis showing the hydrogen bonds.

packing. For ETT-TTF, ETEDT-TTF, and ET-TTF the symmetrical part dominates over the dissymmetrical one (ethylenethio substituent), since all of them have a packing similar to those of the symmetric donors, i.e., DT-TTF, BEDT-TTF, and TTF, that differs completely from the planar sheet motif observed in BET-TTF. In the ETTDM-TTF donor this trend is observed also since the symmetric donor BTDM-TTF (bis(thiodimethylen)tetrathiafulvalene) has a very similar packing[13,23] to that of both ETTDM-TTF and BET-TTF. It is noteworthy that the same packing pattern of ETEDT-TTF has been found in other dissymmetrical derivatives of BEDT-TTF such as DMET and EDT-TTF. In all cases an angular packing is found, with the molecules forming head-to-tail dimers and showing a boat conformation of the six-membered ring. The folding of the donor arises from the energy gained through the formation of intermolecular S···H−C and C···H−C interactions in the dimers.[3]

4. Redox Properties of Donors

In cyclic voltamperometry all donors show two reversible one-electron redox waves, which indicates that they form stable cation radicals and dications. The values of the $E_{1/2}$ potentials in different solvents are given in Table 1 together with those of related compounds. Both $^1E_{1/2}$ and $^2E_{1/2}$ are considerably higher for ETDCM-TTF than for the other donors due to the electron-withdrawing character of the carboxymethyl groups indicating the poor donor properties of this compound. All other compounds can be considered as good donors, with the selenium-substituted TTF derivatives being slightly better than sulfur-substituted ones. All compounds with fused aromatic rings have higher redox potentials than the better donor DS-TTF since the aromaticity of selenophene is not as large as that of thiophene or benzene. As can be observed in Table 1, the values of the redox potentials of the dissymmetric donors are in all cases intermediate between those of the related symmetric ones. All donors with fused thiophene or selenophene rings have small differences between the first and second oxidation potentials ($\Delta E_{1/2}$). This is a good condition for the preparation of molecular conductors since this value is related to the intramolecular electronic repulsion, U. On lowering $\Delta E_{1/2}$, U decreases and the mobility of the electrons increases, resulting in a higher conduction through the solid.

On the other hand, the cation radical derivatives of most of the donors have been generated in solution and studied by UV−vis−NIR and ESR spectroscopy as all of them are fairly stable for days, since the ESR signal intensity does not decrease appreciably.[6,12,13] This characteristic is very important to generate radical−ion salts by electrocrystallization.

5. Molecular Materials: Charge-Transfer Complexes and Radical–Ion Salts

Most of the donors form charge-transfer complexes and radical−ion salts showing, in many cases, good conducting properties. BET-TTF has been the more studied donor even though in many cases BET-TTF-based materials afford poor quality crystals and furthermore lead to the formation of more than one compound from the same experiment. Simple monovalent anions of different geometries as well as other kinds of anions including those with magnetic characteristics have been combined with BET-TTF.

Table 1. Half-Wave Oxidation Potentials[a]

donor	solvent	$^1E_{1/2}$ (V)	$^2E_{1/2}$ (V)	$\Delta E_{1/2}$ (V)	ref
BET-TTF	DMF	0.43	0.58	0.15	6
	MeCN	0.39	0.66	0.27	12
	BzCN	0.36	0.68	0.32	7
BES-TTF	BzCN	0.32	0.66	0.34	7
αDS-TTF	BzCN	0.38	0.71	0.33	7
αDT-TTF	BzCN	0.46	0.79	0.33	7
	DMF	0.50	0.67	0.18	6
BES-TSF	BzCN	0.47	0.74	0.27	7
ETEDT-TTF	CH_2Cl_2	0.47	0.88	0.42	12
	DMF	0.55	0.72	0.16	12
	MeCN	0.43	0.72	0.28	12
ETDCM-TTF	CH_2Cl_2	0.62	1.10	0.47	12
	MeCN	0.58	0.92	0.34	12
ET-TTF	CH_2Cl_2	0.43	0.90	0.47	12
	DMF	0.46	0.67	0.22	12
	MeCN	0.37	0.71	0.33	12
ETT-TTF	DMF	0.64	0.85	0.21	13,24
	MeCN	0.52	0.85	0.30	13,24
ETTDM-TTF	DMF	0.49	0.68	0.21	13,14
	MeCN	0.43	0.73	0.30	13,14
TTF	DMF	0.39	0.62	0.23	29
	MeCN	0.37	0.75	0.38	30
	BzCN	0.34	0.71	0.37	7
BEDT-TTF	DMF	0.63	0.75	0.12	12
	MeCN	0.57	0.83	0.26	30
TCM-TTF	DMF	0.80	1.08	0.28	2d,31
DT-TTF	DMF	0.78	0.96	0.18	6
BTDM-TTF	DMF	0.55	0.72	0.17	6
TSF	BzCN	0.49	0.78	0.29	7

[a] Potentials vs Ag/AgCl; Pt working and counter electrodes.

5.1. From Symmetric Donors

5.1.1. BET-TTF Derivatives

5.1.1.1. Charge-Transfer Complexes. BET-TTF forms by reaction with TCNQ a mixed-valence charge-transfer complex as ascertained by vis−NIR and IR spectroscopy that shows the typical charge-transfer bands and broad a_g modes, whereas with the stronger acceptor $TCNQF_4$ a completely ionic salt is formed.[32,33] The charge transfer was estimated to be 0.5 and 0.95, respectively, based on the position of the CN stretching.[34] It was not possible to obtain single crystals of these compounds by any methodology; therefore, it was impossible to have structural data and good conductivity measurements. The ESR characteristics of the TCNQ complex ($g_{av.} = 2.0047$, $\Delta Hpp = 6$ G) are very similar to the ones of metallic BTDM-TTF:TCNQ complex.[35] The narrow line width points toward a one-dimensional character for the BET-TTF:TCNQ mixed-valence complex.

BET-TTF also form a charge-transfer complex with the poorer acceptor C_{60} but not with C_{70}. In this case, isostructural crystalline ternary complexes were obtained from both toluene and chlorobenzene solutions.[36] Figure 12a shows the crystals structure of the BET-TTF:C_{60}:toluene 1:1:1 ternary complex that is formed by close-packed fullerene sheets parallel to

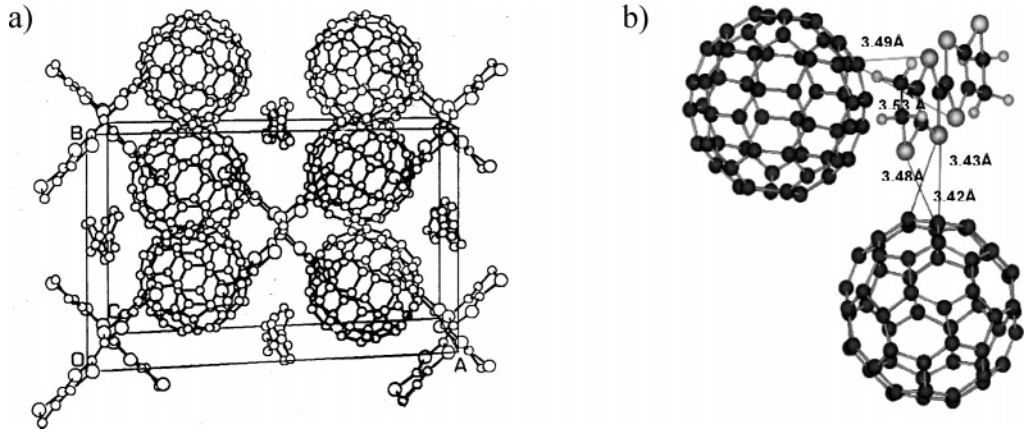

Figure 12. (a) View of the crystal packing of C_{60}:BET-TTF:C_7H_3 along the *c* axis. (b) Closest contacts between C_{60} and BET-TTF.

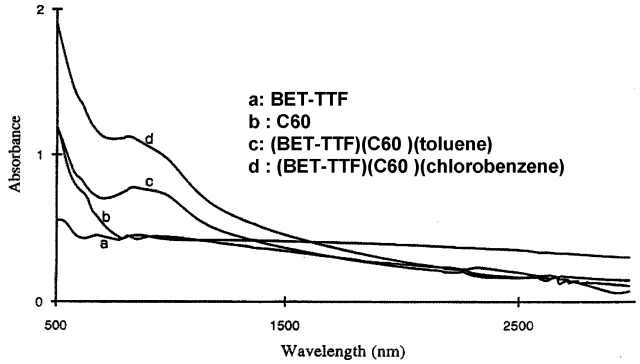

Figure 13. Electronic spectra in KBr pellets.

the *bc* crystallographic plane separated by layers of BET-TTF and disordered toluene molecules along the *a* axis. The packing of C_{60} in these complexes also has been found in many other neutral complexes.[37] BET-TTF donors are the trans isomer and define continuous channels along the *c* axis in which the classical S···S contacts and π overlap of TTF derivatives are absent. By contrast, strong C_{60}−BET-TTF interactions are established through several C(C_{60})···S(BET-TTF) contacts shorter than the sum of the van der Waals radii (Figure 12b).

Both vis−NIR and ESR spectroscopies[36] indicates that there is a small charge transfer between the donor and acceptor even though the difference between the oxidation potential of BET-TTF and the reduction potential of C_{60} is too high to promote charge transfer. In Figure 13 the electronic spectra of both complexes as well as those of the separated components are presented showing clearly that in both complexes a new charge-transfer band appears around 850 nm. The ESR signal parameters of both complexes are also in accord with the existence of interacting C_{60}^{-}· and BET-TTF^{+}· radical species since the *g* values are intermediate to the C_{60} radical anion[38] and the BET-TTF radical cation.[6] The charge transfer can be promoted by the strong interactions revealed in the crystal structure of both complexes.

5.1.1.2. Salts with Linear Anions. It is well known that BEDT-TTF salts containing the linear trihalide anions are one of the most interesting families of molecular materials,[1] with a large variety of physical properties ranging from semiconductors to superconductors and with very interesting phase-transition phenomena.[39]

Attempts to form salts of BET-TTF with several trihalide anions (I_3, I_2Br, IBr_2), either by electrocrystallization or chemical oxidation, resulted in a very low yield of powder materials.[32]

Combination with AuX_2^- (X = Br, I) anions gave a range of mixed-valence compounds as either microcrystalline powders or flakes (very thin platelike crystals).[40] With the AuI_2^- anion three different salts were obtained, namely, (BET-TTF)$_2$AuI_2, (BET-TTF)$_3$-(AuI_2)$_2$, and (BET-TTF)$_m$(AuI_2)$_n$, whereas with the bromine analogue, four different salts with 1:1, 2:1, 3:2, and 4:3 stoichiometry were synthesized. Changes in the experimental conditions permit preparation of the different salts; thus, 1:1 and 2:1 salts were obtained by electrocrystallization, whereas salts with all other stoichiometries result from direct reaction in different solvents. In some cases two or more salts with different stoichiometries grew in the same experiment.

Only for the completely ionic salt (BET-TTF) $AuBr_2$, crystals of enough quality for X-ray structure determination were obtained. Molecules of BET-TTF in the crystal are centrosymmetric and quasi-planar as the trans isomer. In the crystal structure (Figure 14) BET-TTF molecules are tilted stacked along the *c*-axis, with the $AuBr_2^-$ anions located between these stacks which are forming layers by short S···S contacts in the *ab* plane. Noticeably, the arrangement adopted by the donor molecules is very similar to that of neutral BET-TTF.

Interestingly, the ESR properties of all mixed-valence salts (BET-TTF)$_m$(AuX_2)$_n$ (X = Br, I) are very similar showing not only the same parameters at room temperature but also the same variation with the temperature.[40] This fact could indicate that the different salts with the Au_2X linear counterion have a very similar BET-TTF packing arrangement that does not seem to have one-dimensional character owing to the high value of the line width (ΔHpp between 45 and 50 G). The mixed-valence character of all these salts is confirmed by the broad A band shown in their vis−NIR spectra as well as by observation of several vibronic bands (a_g modes) around 1200 and 150 cm^{-1} resulting from electronic-molecular vibration (e-mv) coupling.[41]

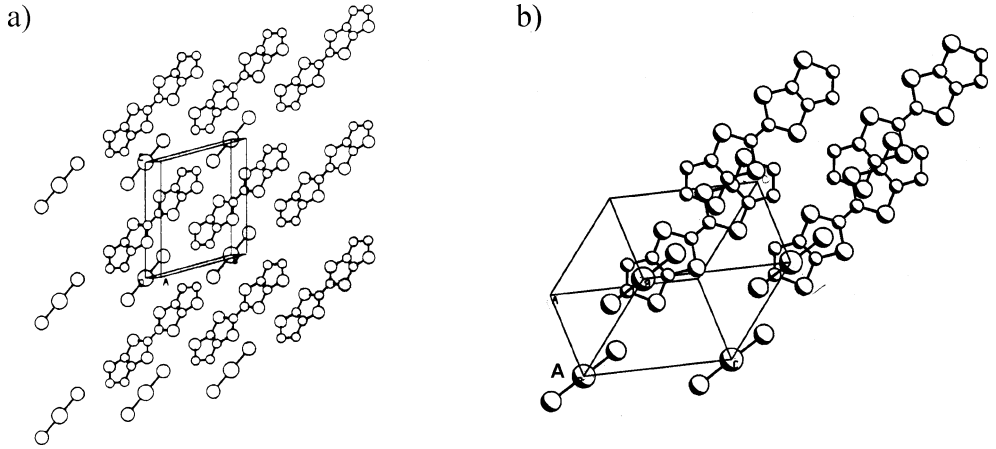

Figure 14. (a) View of the crystal packing of (BET-TTF) $AuBr_2$. (b) View showing the overlap of BET-TTF along the stacks.

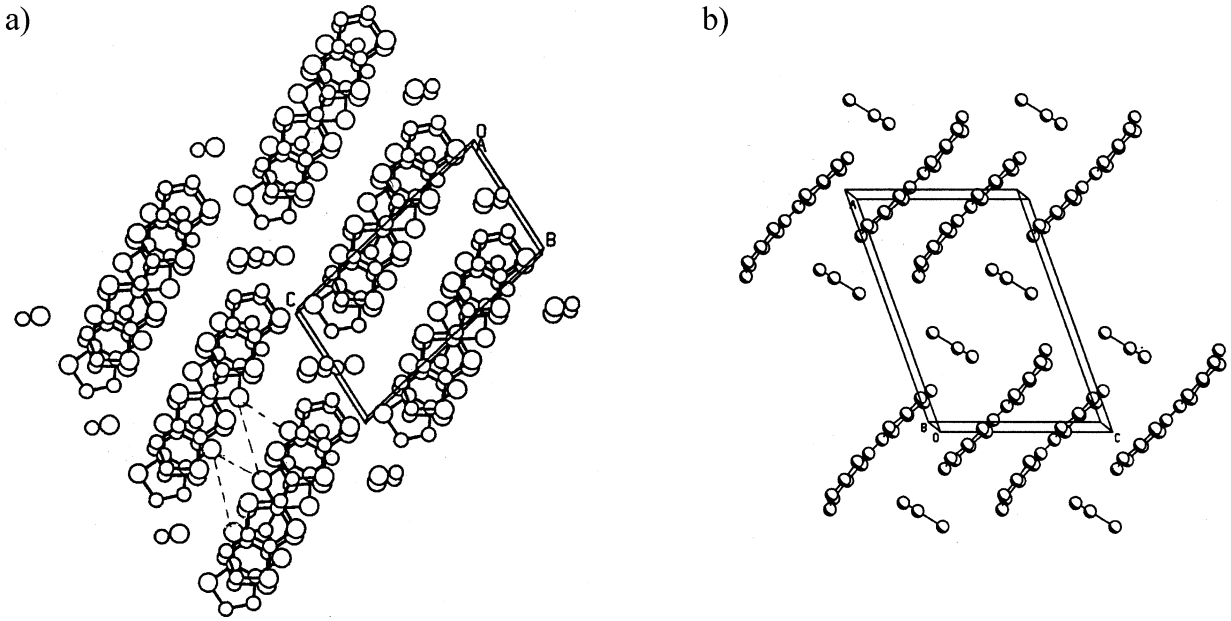

Figure 15. (a) Crystal packing of $(BET\text{-}TTF)_2SCN$. (b) Crystal packing of (BET-TTF)SCN.

Only for $(BET\text{-}TTF)_2AuBr_2$ was it possible to find crystals good enough to perform four-probe dc electrical conductivity measurements, giving a room-temperature conductivity of 1.1 S cm^{-1} with an activated behavior ($\Delta = 0.138$ eV).

So far the best linear anion to be combined with BET-TTF is SCN^-, which gives rise to single crystals of BET-TTF salts by electrocrystallization.[42] In most cases, the pure mixed-valence salt $(BET\text{-}TTF)_2SCN$ was obtained, although in some experiments other crystals with different composition (BET-TTF)SCN and morphology appear. In contrast to the salts derived from AuX_2 anions, both salts can be easily distinguished by means of ESR spectroscopy. Thus, the completely ionic salt has a very narrow and symmetrical line (ΔHpp = 1.1 (*ab*), 1.4 (*c*) G), whereas mixed-valence salt displays a broader signal (6.8 (*a*) 8.3 (*b*) 10.9 (*c*) G) with a Dysonian line shape typical of metals in the *ab* plane (A/B = 2.2).

Crystal structures of both salts are depicted in Figure 15. In both salts the SCN^- counterion has 50% structural disorder and the BET-TTF is also disordered (25% in the 2:1 salt and 50% in the 1:1 salt). Interestingly, the X-ray data clearly reveal the presence of the cis isomer of BET-TTF in the mixed-valence salt, although the starting BET-TTF was the trans isomer. It is therefore clear that a trans−cis isomerization takes place during electrocrystallization as already observed in other cyclic substituted donors.[43]

The crystal packing of $(BET\text{-}TTF)_2SCN$ is β type, with BET-TTF molecules forming zigzag chains along the *a* axis interacting in the *bc* plane (Figure 15a). Sheets of donors and anions alternate along the *c* axis. It is interesting to point out that although $(BET\text{-}TTF)_2SCN$ is structurally a typical β-type salt, its Fermi surface is open (Figure 16), which confers a 1D electronic character to this salt.

Despite the structural disorder, crystals of $(BET\text{-}TTF)_2SCN$ show metallic behavior down to 60 K and then resistance increases slowly down to 4 K (Figure 17). In agreement with the electronic structure and the ESR studies the conductivity in the *ab* plane is 10^2 higher than that in the perpendicular direction. Application of pressure increases, as expected, the conductivity but does not destroy the transition

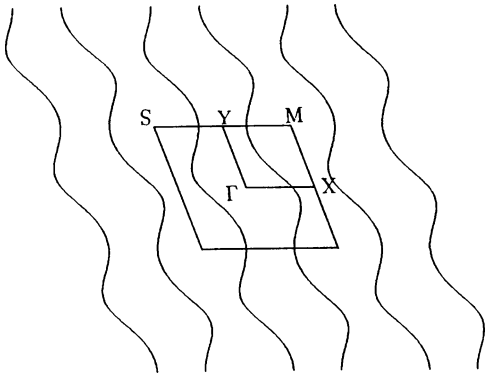

Figure 16. Calculated Fermi surface for (BET-TTF)$_2$SCN.

(Figure 17b).[44,13] This can account for the disorder in the structure that promotes localization of electrons in the defects.

5.1.1.3. Salts with Tetrahedral Anions. Different tetrahedral anions, as ClO_4, BF_4, ReO_4, and MX_4 (M= Fe, Ga; X = Cl, Br), have been used to grow salts with BET-TTF. By far the most interesting results were obtained with ReO_4 and the magnetic anion $FeCl_4$.

Small variation of solvent polarity in the electrocrystallization of BET-TTF donor with ^{n}Bu$_4$NReO$_4$ as supporting electrolyte allows the formation of three different salts, (BET-TTF)ReO$_4$, (BET-TTF)$_3$(ReO$_4$)$_2$, and (BET-TTF)$_9$(ReO$_4$)$_4$·2THF, the last one being the only BET-TTF derivative that incorporates the organic solvent used for electrocrystallization in the crystal structure.[45,46] There are some similarities between these salts and the ones obtained with the ReO_4^- anion and the BEDT-TTF donor, for which several 3:2 phases as well as a mixed-valence salt containing THF, (BEDT-TTF)$_2$ReO$_4$·0.5THF, are known.[47] Nevertheless, whereas for (BEDT-TTF)$_3$(ReO$_4$)$_2$ three different crystallographic phases (α, β, and γ) and for the salts with a 2:1 stoichiometry two phases have been obtained,[47,48] only one crystallographic phase of the (BET-TTF)$_3$(ReO$_4$)$_2$ and (BET-TTF)$_9$(ReO$_4$)$_4$·2THF salts has been discovered so far.

Concerning the crystal structures, in the completely ionic salt BET-TTF stacks in a parallel fashion different from the other 1:1 salts of BET-TTF. The stacks, running along the *a* direction, are not regular but form weak dimers (Figure 18a). (BEDT-TTF)$_3$(ReO$_4$)$_2$ salt has a very interesting crystal composition since it is configured by two different radical cation layers (Figure 18b), and analysis of the bond length of BET-TTF molecules forming layers 1 and 2 shows that the β-like layer 1 has mixed-valence character while layer 2 can be regarded as an anion−cation−anion [ReO$_4$(BET-TTF)ReO$_4$]$^-$ sandwich layer with completely ionized BET-TTF. In this layer the (BET-TTF)$^{1+}$ radical cations are practically not interacting with each other. However, there is a pronounced interaction between (BET-TTF)$^{1+}$ and ReO_4^- since every cation II has 12 short S···O and C···O contacts with the anion. On the other hand, (BET-TTF)$_9$(ReO$_4$)$_4$·2THF is formed by only one β-like layer that consists of two different mixed-valence stacks (Figure 18c)

As in some previous examples, there is positional disorder in the sulfur atoms of the external rings of BET-TTF molecules of the three salts. From the study of the occupation factors of the corresponding sulfur and carbon atoms it is only possible to conclude that the BET-TTF molecules of type II in (BET-TTF)$_3$(ReO$_4$)$_2$ salt and the BET-TTF molecules of type I in (BET-TTF)$_9$(ReO$_4$)$_4$·2(THF) salt have a *trans*-configuration.[45]

The Fermi surface of layer 1 of (BET-TTF)$_3$(ReO$_4$)$_2$ is open and very similar to that of the (BET-TTF)$_2$SCN salt in accordance with their very similar packing (Figure 19a). The Fermi surface of salt (BET-TTF)$_9$(ReO$_4$)$_4$·2THF (Figure 19b) contains closed sections with a cross-sectional area of 14.8% of the Brillouin zone around Γ (hole pockets) and M (electron pockets). The shape of the Fermi surface is not changed when the outer five-membered rings are

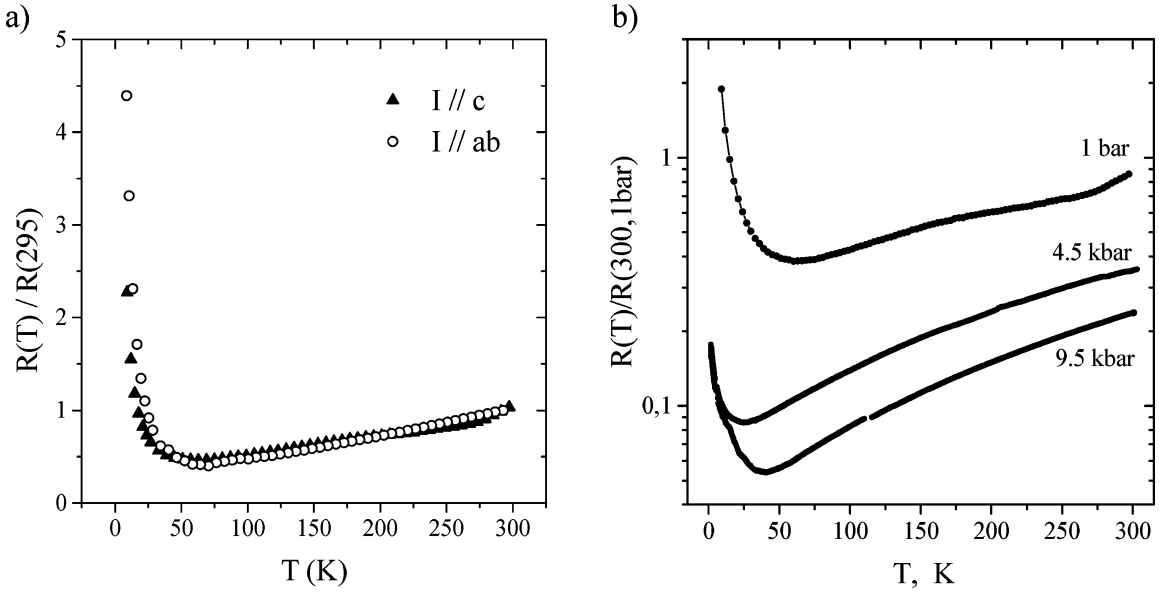

Figure 17. (a) Temperature dependence of normalized resistance for a representative crystal of (BET-TTF)$_2$SCN. (b) Normalized resistance versus temperature at different pressures.

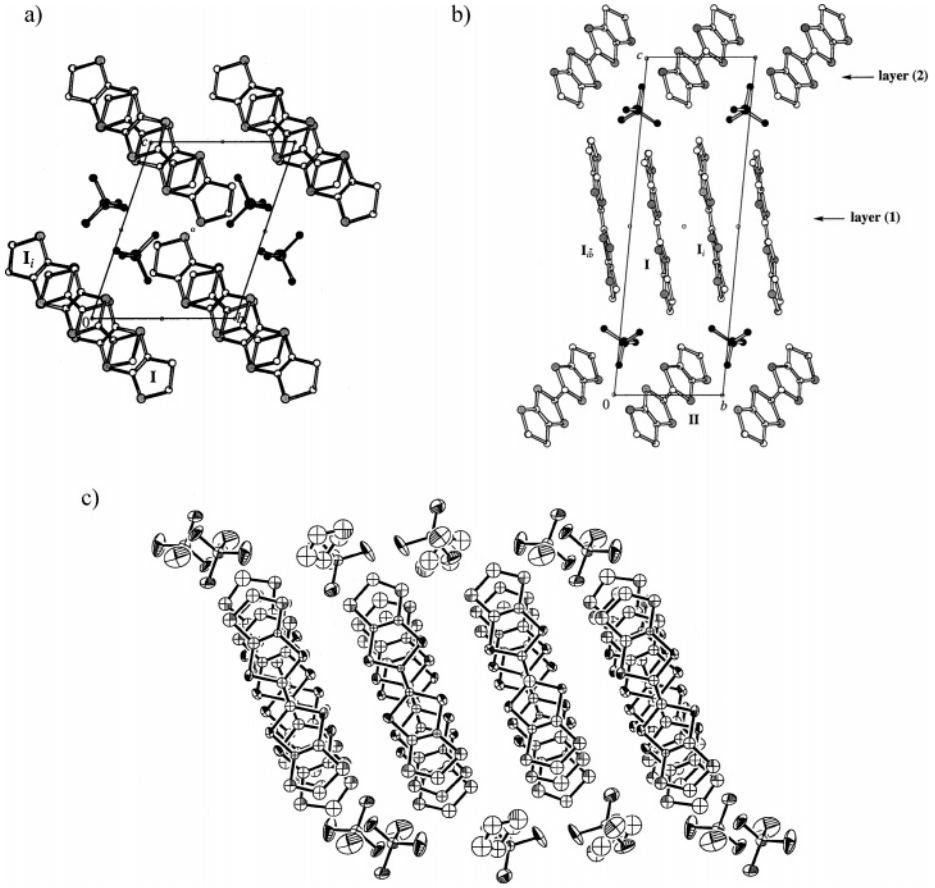

Figure 18. Crystal packing of (a) (BET-TTF)ReO_4, (b) (BET-TTF)$_3(ReO_4)_2$, and (c) (BET-TTF)$_9(ReO_4)_4$·2THF.

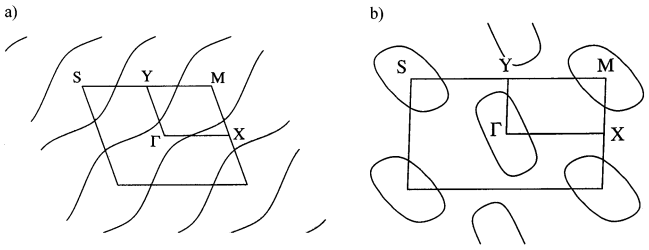

Figure 19. Fermi surface of (a) layer I of (BET-TTF)$_3$-$(ReO_4)_2$ and (b) (BET-TTF)$_9(ReO_4)_4$·2THF.

disregarded in the calculations, the disorder of the donor lattice playing a very minor role in the electronic structure of these salts.

In agreement with the results from X-ray structure determination and electronic structure calculations, the mixed-valence salts (BET-TTF)$_3(ReO_4)_2$ and (BET-TTF)$_9(ReO_4)_4$·2THF exhibit metallic character down to 125 and 75 K, respectively. In fact, the properties of (BET-TTF)$_3(ReO_4)_2$ should be compared with those of the family of salts (BET-TTF)$_2$X (X = PF_6, AsF_6, SbF_6, TaF_6, and SCN) because their conducting layers have the same composition $[(\text{BET-TTF})^{0.5+}]_2$ and packing (β type). Interestingly, a first-order phase transition at high pressure (P = 4−5 kbar) has been observed for the (BET-TTF)$_9(ReO_4)_4$·2THF.

Regarding its magnetic properties, the (BET-TTF)$_3$-$(ReO_4)_2$ salt is the most interesting one. This salt contains delocalized conduction electrons as well as localized magnetic moments located in the two different layers of donors that constitute the salt. The ESR study of this salt indicates that both kinds of electrons are interacting.

To prepare new materials such as the previous one containing both localized moments and conducting electrons, combination of BET-TTF with tetrahedral magnetic anions as $[FeX_4]^-$ (X = Cl, Br) is very interesting.

Isostructural (BET-TTF)$_2[MCl_4]$ (M = Fe, Ga) salts having paramagnetic and diamagnetic anions were obtained by electrocrystallization.[49] The corresponding Br-containing salts have been also prepared, although the crystals are of poor quality. Nevertheless, the optical and electrical properties are very similar to their Cl counterparts, pointing toward isostructural compounds.[11]

The structure of the (BET-TTF)$_2[MCl_4]$ salts (Figure 20) consists of layers of donor molecules which are interweaved by the organic anions. There are two crystallographically independent molecules, each one forming a different type of layer (I and II in Figure 20). Layers I are identical to that found in the λ-phase of (BETS)$_2FeCl_4$ studied by Kobayashi et al.,[50,51] molecules forming zigzag-connected chains. In layers II the BET-TTF molecules form chains with an almost eclipsed stacking. The inorganic anions are located in the holes created by the zigzag chains in such a way that they are fairly well isolated from each other but connected through S···Cl and C···Cl short contacts with the donors.

No disorder was observed in the trans isomer of BET-TTF forming the structure, although two of the

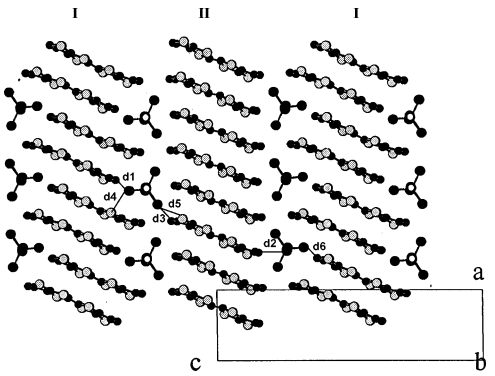

Figure 20. View of the crystal structure of (BET-TTF)$_2$GaCl$_4$ in the *ab* plane showing the two different kinds of organic layers (I and II). Shortest anion−donor distances are also depicted.

chlorine atoms of the $GaCl_4$ anion were disordered over two sites.

In accordance with their crystal packing and electronic spectra (which show an intense A band and a_g modes), both Cl salts and $GaBr_4$ salt are metals with moderate room-temperature conductivity (around 50 S cm^{-1}). As observed in other metallic salts of BET-TTF, at low temperatures (T < 25) a smooth increase of resistivity due to localization effects takes place. Crystals of the (BET-TTF)$_2$GaCl$_4$ salts have been studied under pressure, and although the localization of the electrons is almost suppressed at 11 kbar, no superconducting transition was observed.[44]

Magnetic susceptibility measurements on the (BET-TTF)$_2$FeCl$_4$ salt indicate a moderate Fe−Fe interaction (J/k = −0.22 K) that is at least 1 order of magnitude larger that the dipolar Fe−Fe interactions estimated from the crystallographic distances. A plausible mechanism to account for this interaction would involve coupling of the localized spins with the conduction electrons since numerous strong anion−donor contacts exist in the crystal. Such an assumption is supported by the ESR measurements. Thus, a single broad signal of ca. 400 G at room temperature and centered at g = 2.0017 is observed in the whole temperature range (300−4 K), indicating the presence of magnetic interactions between both sublattices.

5.1.1.4. Salts with Octahedral Anions. Since changes in the anion geometries can induce changes in the properties of the obtained materials as well as a better tendency to crystallize, combination of BET-TTF with octahedral anions that have been very fruitful with other donors is a good choice to achieve materials with good properties.

As in the case of linear and tetrahedral anions, when BET-TTF was combined with the octahedral XF_6^- anions (X = P, As, Sb, Ta), salts with different stoichiometry were obtained only with small changes in experimental conditions.[52] With all anions the 2:1 phase was the most common one. The completely ionic salt was only obtained using the TaF_6^- anion, and with AsF_6^- and PF_6^- nonstoichiometric phases, namely, (BET-TTF)$(XF_6)_{0.7\pm\delta}$, were also prepared.

It is interesting to point out that the crystal packing of BET-TTF molecules in the (BET-TTF)-TaF_6 salt (Figure 21) is the same found as that in the 1:1 salt with the linear anion $AuBr_2^-$, which in turn is very similar to that presented by the neutral donor. The donors in the crystal are the trans isomer and are completely ordered.

All 2:1 salts are isostructural, and as expected, an increase in the cell volume is observed with an increase of the anion size.[52] Layers of anions and donors with β-type packing alternate along the *b* axis (Figure 22). Within the stacks along the *b* axis, donors are slightly dimerized, and molecules in parallel stacks are interacting in the *ac* plane through short S···S contacts that involve all sulfur atoms of BET-TTF and generate a 2D crystal structures. In contrast with the completely ionic (BET-TTF)TaF_6 salt, donors are disordered in all structures.

Despite this characteristic, all (BET-TTF)$_2XF_6$ (X = P, As, Sb, and Ta) salts display metallic properties very similar to that of the (BET-TTF)$_2$SCN salt, thus presenting a smooth metal−semiconductor transition at temperatures between 150 and 75 K and

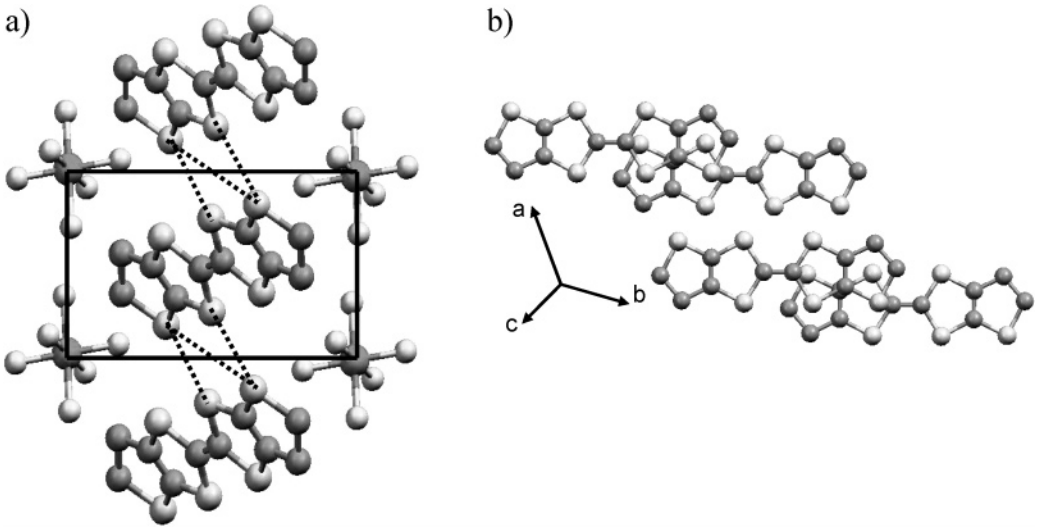

Figure 21. Crystal packing of (BET-TTF)TaF_6 showing (a) the alternating layers of donors and anions along the *c* axis and (b) the donor overlap within the stacks

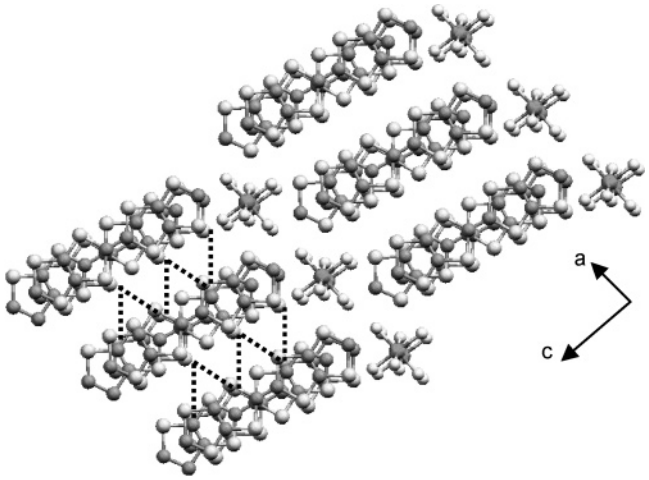

Figure 22. Crystal packing of $(BET\text{-}TTF)_2TaF_6$ showing the S···S interstack contacts as dashed lines.

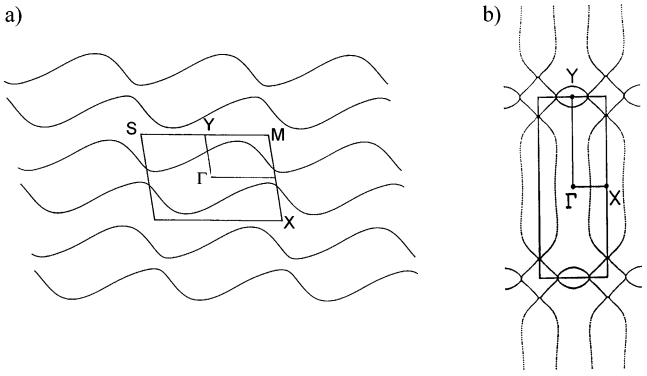

Figure 23. Calculated Fermi surface of (a) $(BET\text{-}TTF)_2SbF_6$ and (b) (BET-TTF) $(PF_6)_x$ assuming $x = 2/3$.

having room-temperature conductivities between 300 and 100 S cm^{-1}.[52]

Tight-binding band calculations lead to the conclusion that both the band structures and the Fermi surface of these β-type salts are not strongly affected by the existence of disorder, although this disorder has an important role in forcing the loss of metallic character at low temperature. The Fermi surface lies at the boundary between 1D and 2D systems, which accounts for the 1D characteristic of the ESR parameters and with the 2D structural character. The Fermi surface for the donor slabs of $(BET\text{-}TTF)_2SbF_6$ assuming no disorder is shown in Figure 23a.

On the other hand, the crystal packing motif of the isostructural salts $(BET\text{-}TTF)(XF_6)_{0.7}$ (X = P, As) is very similar to the α-phases of BEDT-TTF,[1] with uniform stacks of BET-TTF in a herringbone pattern forming sheets that alternate with disordered anions along *c* (Figure 24). The calculated Fermi surface, assuming a 1:2/3 stoichiometry, consists of a closed loop with an area of four-thirds of the first Brioullin zone (Figure 23b).

The electrical properties of the $(BET\text{-}TTF)(XF_6)_{0.7}$ salts are quite interesting, showing an unusual behavior (Figure 25). The resistance increases slowly down to 120 K, a change in slope taking place around 200 K. With further cooling a metallic behavior is observed down to 50 K, where a transition to a semiconductor state occurs. Conductivity at room temperature is around 15 S cm^{-1} and is quite isotropic in the *ab* plane, in accordance with the Fermi surface. A possible explanation for this peculiar behavior relies on the anion deficiency and disordering. Partial ordering of the anions can lead to the observed metallic behavior but apparently cannot prevent further localization at lower temperatures.

The ESR characteristics of these salts with octahedral anions are in accordance with their different crystal packing and electronic dimensionality, with the line width values of the quasi-2D β-type 2:1 salts (between 8 and 14 G) being lower than those of the α-type $(BET\text{-}TTF)(XF_6)_{0.7}$ salts (between 28 and 48 G), which have closed Fermi surfaces.[52,53] Also, variation of the ESR parameters on rotating the crystals of the $(BET\text{-}TTF)(XF_6)_{0.7}$ salts shows isotropic behavior in the *ab* plane in accordance with the transport properties and Fermi surface.[54]

Other very interesting anions with the same octahedral shape, although with different charge, are the paramagnetic hexacyanoferrate(III) $[Fe(CN)_6]^{3-}$ anion and the nitroprusside anion $[Fe(CN)_5NO]^{2-}$. These anions, combined with BET-TTF which forms conducting layers in the crystals, open the possibility of combining conductivity and magnetism and conductivity and optical properties in the same material. This approach of combining metallic layers (mobile electrons) and magnetic anions (localized electrons) as well as mobile electrons with the optical properties derived from photochromic nitroprusside anions[55] has

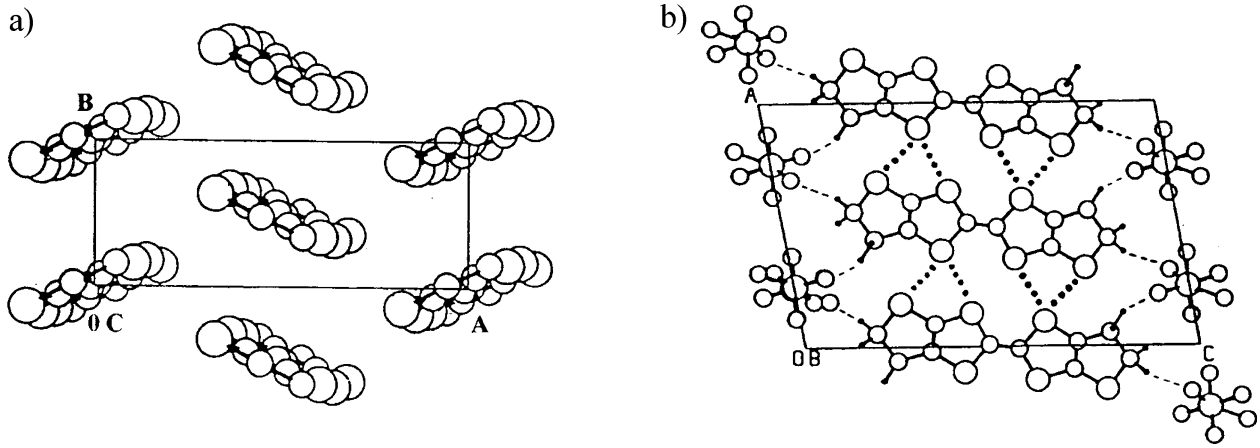

Figure 24. Crystal structure of $(BET\text{-}TTF)(PF_6)_{0.7}$. (a) Projection of the donors layer along *c*. (b) Projection in the *ac* plane showing close intermolecular contacts (S···S < 3.68 Å; F···H < 2.55 Å).

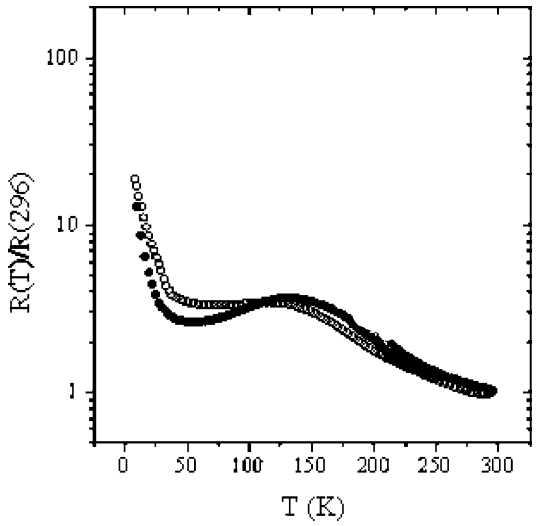

Figure 25. Resistance vs temperature of (BET-TTF)-$(PF_6)_{0.7}$ (●) and (BET-TTF)$(AsF_6)_{0.7}$ (○).

already led to the preparation of many molecular materials with extremely interesting properties.[56,57]

Combination of the donor molecule BET-TTF with the octahedral anions $[Fe(CN)_6]^{3-}$ and $[Fe(CN)_5NO]^{2-}$ has given rise to two radical salts formulated as $(BET\text{-}TTF)_4(NEt_4)_2[Fe(CN)_6]$ and $(BET\text{-}TTF)_2[Fe(CN)_5NO]\cdot CH_2Cl_2$.[58] Even if both anions are very similar in shape and size, the two salts have very different stoichiometries, packing motifs, and oxidation states of the donors that in turn are also completely different from those with the previous octahedral monoanions. Thus, the structure of $(BET\text{-}TTF)_4(NEt_4)_2[Fe(CN)_6]$ salt consists of layers of the organic donors alternating along the *a* axis with layers formed by the hexacyanoferrate anions and NEt_4^+ cations. The organic layer contains only one crystallographically independent BET-TTF molecule that is packed in orthogonal dimers, forming the unique κ-phase observed in a crystal derived from this donor (Figure 26a). Analysis of the bond distances and the electronic and IR spectra suggests a degree of ionicity of 1/4 per BET-TTF molecule, in agreement with the stoichiometry of the salt.

Donor molecules in the $(BET\text{-}TTF)_2[Fe(CN)_5NO]\cdot CH_2Cl_2$ salt also form dimers but have an unprecedented packing of the organic molecules that form zigzag tunnels where the anions and the solvent molecules are located (Figure 26b). The stoichiometry indicates that all BET-TTF molecules are completely ionized. These differences can be attributed, on one hand, to the different anionic charge and, on the other, to the different synthetic strategy used for each salt. Thus, the use of low soluble salts of the anion give rise to high oxidation states (+1) in the organic donor of $(BET\text{-}TTF)_2[Fe(CN)_5NO]\cdot CH_2Cl_2$ as a consequence of the high applied potentials during electrooxidation of the donor.[58,59] For the synthesis of $(BET\text{-}TTF)_2(NEt_4)_2[Fe(CN)_6]$ a very soluble salt of the anion, $(NEt_4)_3[Fe(CN)_6]$, was used, and the oxidation state of the donor in this salt was much lower (1/4).

The electrical properties show that the mixed-valence salt $(BET\text{-}TTF)_4(NEt4)_2$ $[Fe(CN)_6]$ is a semiconductor with a high room-temperature conductivity (11.6 S cm^{-1}) and a low activation energy (45 meV), in agreement with the band structure calculations that show a narrow band with a bandwidth that is somewhat lower than the lowest values calculated for the known metallic κ-phases. This suggests a strong tendency for this salt toward localization and thus activated conductivity, which is quite common for κ-phases. In the present case both the disorder in the donor layer and the lower number of holes (i.e., the average charge of the donors is +1/4 here but +1/2 in the usual κ-phases) makes such localization even more likely.

The magnetic susceptibility of $(BET\text{-}TTF)_4(NEt_4)_2$-$[Fe(CN)_6]$ shows no interaction between both sublattices in the crystal, and besides the paramagnetic contribution from the anion, a temperature-independent paramagnetism (TIP) of Pauli type, due to electronic delocalization observed at high tempera-

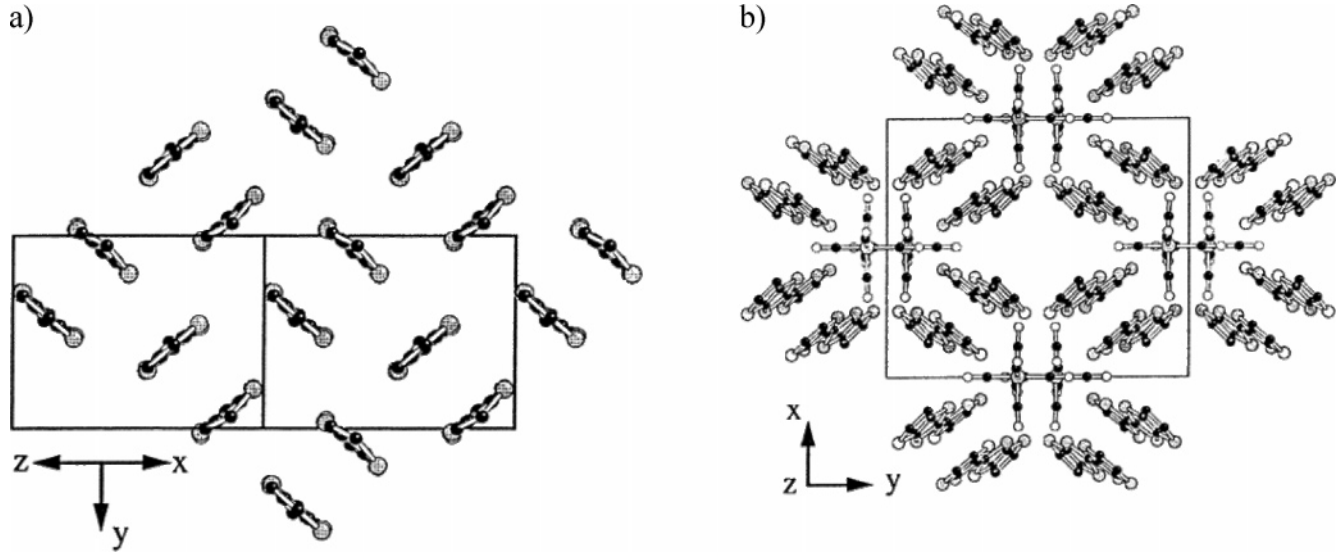

Figure 26. (a) View of the crystal packing of the donor layer in $(BET\text{-}TTF)_4(NEt_4)_2[Fe(CN)_6]$ along the longest axis of BET-TTF molecules showing the κ-type packing of the donor layer. (b) $(BET\text{-}TTF)_2[Fe(CN)_5NO]\cdot CH_2Cl_2$ along *c* showing the channels created by the BET-TTF dimers (included solvent has been omitted for clarity).

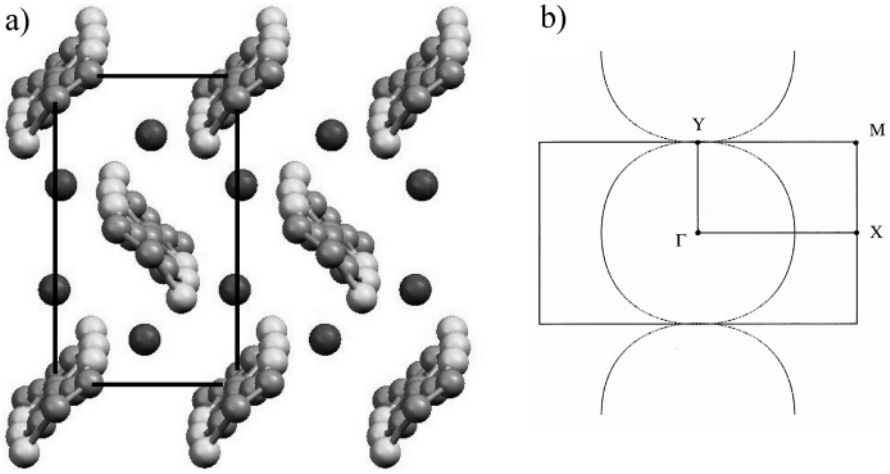

Figure 27. (a) Crystal packing of $(BET\text{-}TTF)_2Br{\cdot}3H_2O$ along the *c* direction. (b) Calculated Fermi surface for the BET-TTF slabs of $(BET\text{-}TTF)_2Br{\cdot}3H_2O$.

tures in the organic sublattice, is observed. This Pauli-type paramagnetism is confirmed by the ESR spectra that also show a Dysonian line when the magnetic field is parallel to the conducting plane, typical of metallic and highly conducting systems. On the other hand, the completely ionic salt $(BET\text{-}TTF)_2[Fe(CN)_5NO]{\cdot}CH_2Cl_2$ behaves as a semiconductor with a very low room temperature conductivity. The magnetic properties of this salt indicate that the unpaired electrons on the organic molecules are strongly antiferromagnetically coupled, giving rise to a diamagnetic behavior as the nitroprusside anion is also diamagnetic.

5.1.1.5. Salts with Monatomic Anions. Since the Fermi surface of the $(BET\text{-}TTF)_2XF_6$ salts is almost closed, we believe that by inducing a closer packing (chemical pressure) through the use of smaller anions the Fermi surface can be closed, giving rise to 2D band structures very similar to that of the superconducting BEDT-TTF β salts. For this reason the monatomic anions, Br^- and Cl^-, that have the additional advantage of their symmetry, which prevents the possibility of being disordered, were combined with BET-TTF.

Electrocrystallization of BET-TTF with the tetrabutylammonium salts of Br^- and Cl^- anions gave isostructural hydrated mixed-valence salts with formula $(BET\text{-}TTF)_2X{\cdot}3H_2O$ (X = Br, Cl) either in the form of needles or almost transparent plates.[60] The crystal structure (Figure 27a) is characterized by θ-type layers[61] of ordered trans isomer of the BET-TTF radical cation alternating along *a* with honeycomblike polymeric anion networks. These are the unique mixed-valence salts derived from BET-TTF that have ordered donors in the crystal structure. The calculated Fermi surface for the Br-containing salt (Figure 27b) indicates a completely 2D electronic structure, and the shape remains when calculated for different values of band filling. This result is relevant in view of the possibility that some of the water molecules are indeed protonated, as found in the case of $(BEDO\text{-}TTF)_2Cl_{1.28}(H_3O)_{0.28}{\cdot}2.44H_2O$.[61b]

The in-plane (*ab* plane) room-temperature conductivity of the BET-TTF halides is very high, varying between 400 and 3900 S cm^{-1} depending on the

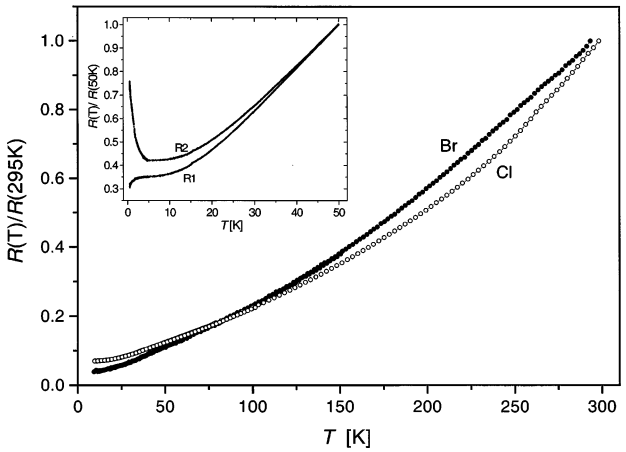

Figure 28. Temperature dependence of the normalized resistance for $(BET\text{-}TTF)_2X{\cdot}3H_2O$ (X = Br, Cl) salts. Inset shows the typical low-temperature behavior of the crystals of the Br-containing salt with some localization effect (R_2) and with a hint of a superconducting transition (R_1).

quality of the samples. The temperature dependence of the resistivity (Figure 28) reveals that these salts are stable metals down to very low temperature (2−6 K), where a small localization effect is observed for most of the crystals. Nevertheless, two of the $(BET\text{-}TTF)_2Br{\cdot}3H_2O$ crystals exhibited typical metallic behavior down to 0.5 K. Moreover, a very pronounced acceleration of the resistance decrease below 2 K was also found, which suggests the onset of a superconducting transition (inset in Figure 28, curve R1).

In accordance with the metallic properties and the 2D electronic character, the intensity of the ESR signal follows a Pauli-like behavior with the temperature and the signal (ΔHpp and *g* values) is isotropic in the *ab* plane.

5.1.1.6. Salts from Dithiolate Complexes. When BET-TTF is combined with planar anions with similar size and shape, as are dithiolate complexes $M(mnt)_2$ (M = Au, Pt)[62] or $Au(i\text{-}mnt)_2$,[63] layers of donors are not developed due to the influence of the anions. With the isomeric anions $Au(mnt)_2$ and $Au(i\text{-}mnt)_2$ mixed stacks are formed, but while $Au(mnt)_2$ forms a completely ionic complex,[62] the isomeric anion develops a mixed-valence salt.[63]

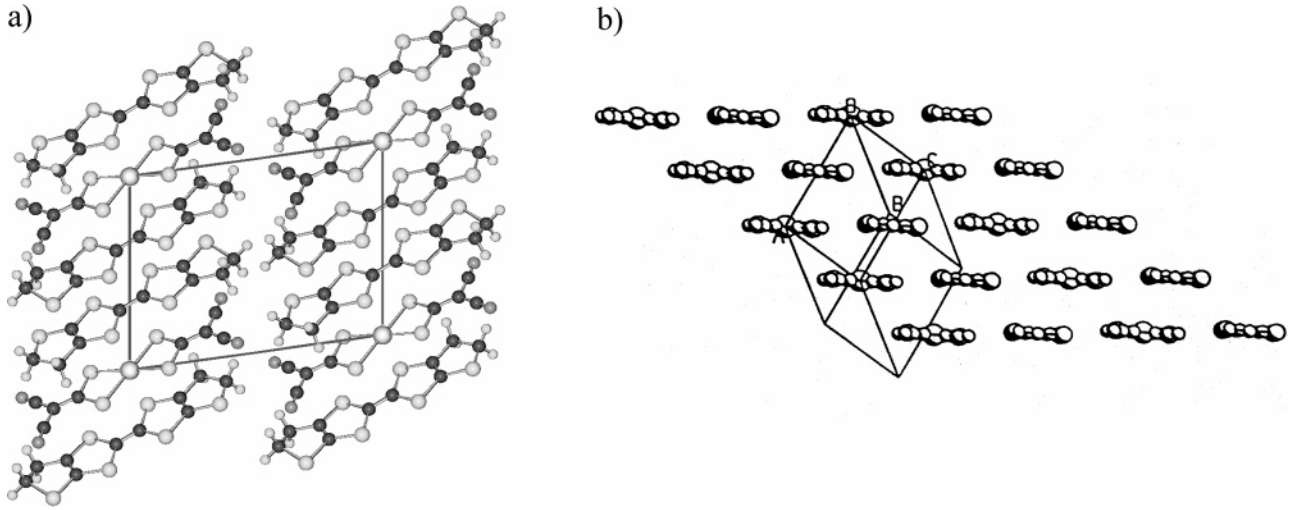

Figure 29. (a) View of the projection on the *ac* plane of the crystal packing of (BET-TTF)$_2$Au(i-mnt)$_2$. (b) View of the crystal packing of (BET-TTF)Au(mnt)$_2$ parallel to the molecular plane of BET-TTF.

The crystal structure of [BET-TTF]$_2$[Au(i-mnt)$_2$] consists of a parallel arrangement of mixed stacks where acceptors, A, alternate with head-to-tail pairs of donors, DD, ADDADDA (Figure 29a). The stacking direction corresponds to [1−1 0]. Short interchain acceptor−donor and donor−donor S···S contacts were observed. Due to short interchain S···S contacts (AD and DD), a 2D network in the *ab* plane is formed. Interestingly, this is an ordered structure containing the cis isomer of BET-TTF in the crystal. This isomer allows the strong pairing of donors by four short S···S interactions. In fact, this is the only known compound derived from BET-TTF in which unambiguously the cis isomer has been observed as the unique component.

The salt [BET-TTF][Au(mnt)$_2$] also has a completely ordered structure, having one-half of the BET-TTF molecule and one-half or the anion in the asymmetric unit. Nevertheless, by contrast with the salt formed with the isomeric counterion Au(i-mnt)$_2$, in this case the component of the crystal is the trans isomer, which forms mixed stacked DADA columns along the *a* direction (Figure 29b). As in the previous salt, the stacks are bound together by a network of short S···S contacts between adjoining BET-TTF and Au(mnt)$_2$ molecules.

Molecules of BET-TTF in both compounds are tightly bound by neighboring Au(mnt)$_2$ and Au(i-mnt)$_2$ anionic molecules, not only through S···S contacts but also through short contacts between the N atom of the CN groups in the anion and the H atoms of the CH_2 groups in the donor. This can be the cause of the completely ordered BET-TTF, either cis or trans isomers, molecules in the structures.

It is noticeable that mixed-stacked packing has also been observed in other salts with dithiolate complexes as (BEDT-TTF)$_2$[Au(i-mnt)$_2$][64] and (perylene)-Pt(mnt)$_2$.[65]

The transport properties, conductivity, and thermopower of [BET-TTF]$_2$[Au(i-mnt)$_2$] and (BET-TTF)-[Au(mnt)$_2$] reveal a semiconductor behavior with conductivity values at room temperature of 6.6×10^{-2} and 8×10^{-3} S cm^{-1}, respectively. This behavior is in accordance with the low delocalization of the electrons due to the mixed-stacking crystal packing.

Another salt of this family with completely ionic character (BET-TTF)$_2$Pt(mnt)$_2$ in which the Pt complex is a dianion was obtained by charge transfer between the neutral BET-TTF donor and the tetrabutylammonium salt of the monoanion. The diamagnetic character of the anion was confirmed by ESR spectroscopy, which shows a signal typical of the TTF anion radicals.[63]

5.1.1.7. Salts with Polyoxometalate Anions. Polyoxometalate anions, due to their extremely versatile functionality, have been used to prepare numerous molecular-based materials.[66] By combination with TTF derivatives, following the so-called hybrid approach, many materials combining electric and magnetic properties have been developed.

BET-TTF has also been combined with the Lindquist anion $[Mo_6O_{19}]^{2-}$ (M ≃ W and Mo), where anion crystallizes better with other TTF derivatives, and crystalline 2:1 salts of these anions have been obtained.[67]

In the crystal structure face-to-face (BET-TTF$^{+\bullet}$)$_2$ dimers are formed by short S···S contacts, and these dimers are surrounded by polyanions, giving rise to an unusual 3D packing of cations and anions reminiscent of NaCl (Figure 30). This kind of packing with dimerization of the completely charged donors does not favor conductivity and as consequence both displays very low conductivity values at room temperature (3.2×10^{-6} S cm^{-1}).

A radical salt has also been obtained with the silicododecatungstenate $[SiW_{12}O_{40}]^{4-}$ which can be formulated as [BET-TTF]$_4$[$SiW_{12}O_{40}$]·CH_3CN·$2H_2O$. Although a complete structural characterization was prevented due to the poor quality of the crystals, some structural features were evidenced in the X-ray study. Thus, BET-TTF radical cations are also dimerized in this salt, and the anions form a 2D hexagonal packing in the *ab* plane.

5.1.2. BES-TTF, BES-TSF, and DS-TTF Derivatives

5.1.2.1. Charge-Transfer Complexes. BES-TTF and DS-TTF form 1:1 mixed-valence complexes with TCNQ acceptor that can be obtained as single crystals by diffusion method.[7,68] The two complexes have

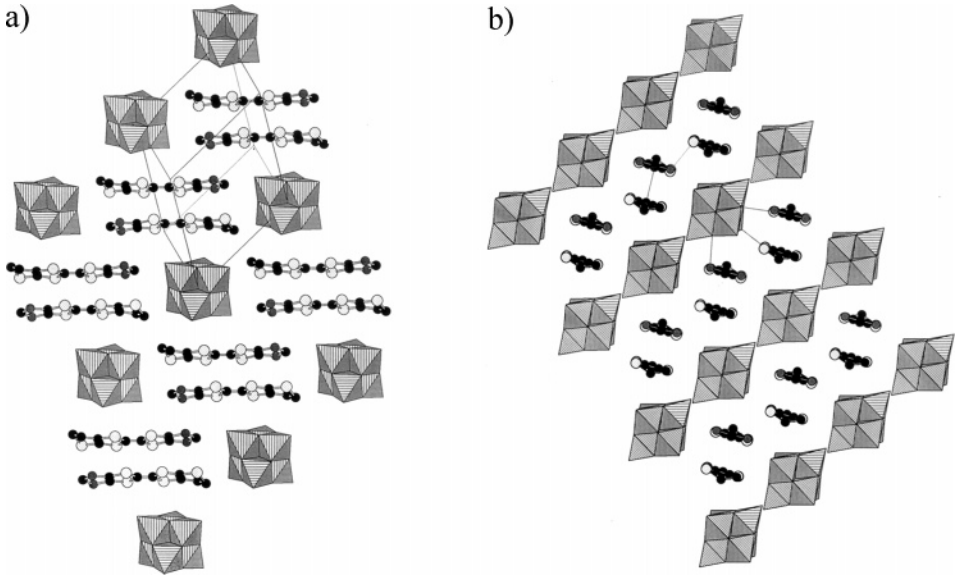

Figure 30. Crystal structure of the 2:1 radical salts of BET with Lindqvist anions, $[BET]_2[M_6O_{19}]$ (M = W, Mo): (a) View in the $(10\bar{1})$ plane showing the 3D organic/inorganic packing. (b) View in the (012) plane showing the contacts between $(BET^{\bullet+})_2$ dimers in the a direction.

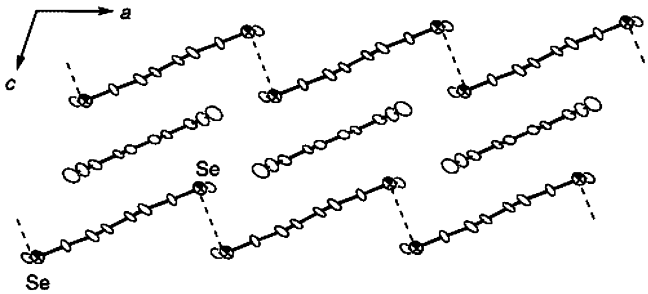

Figure 31. Crystal packing of αDS-TTF:TCNQ.

different crystal structures and physical properties. Thus, whereas DS-TTF:TCNQ is characterized by a mixed-stacking arrangement (Figure 31), BES-TTF:TCNQ shows segregated stacked columns in an angular fashion (Figure 32). BES-TTF molecules in uniform stacks are connected by short Se···Se contacts (3.84 Å) with molecules in neighboring stacks forming a 2D packing similar to the one shown by β phases of BEDT-TTF and BET-TTF salts. As in the crystal structures of BET-TTF derivatives, donor molecules have disorder in the external Se atom.

The electrical properties of both compounds are in accordance with their crystal packing since DS-TTF:TCNQ is a semiconductor whereas BES-TTF:TCNQ has a good room-temperature conductivity (150 S cm^{-1}) and metallic behavior down to 110 K, where a typical metal-to-insulator transition occurs (Figure 33). The high conductivity and low activation energy ($\sigma_{300} = 0.2$ S cm^{-1}; $E_a = 0.064$ eV) shown by the DS-TTF:TCNQ complex displaying a mixed-stack arrangement can be rationalized by the existence of Se···Se interactions (3.80 Å) between donors along the a axis (see Figure 31).

On the other hand, BES-TSF also forms a charge-transfer complex with TCNQ of unknown structure showing a very high room-temperature conductivity of 2700 ± 500 S cm^{-1} and metallic behavior down to 40 K, where a very smooth decrease of conductivity is observed. At 4.2 K the conductivity still remains

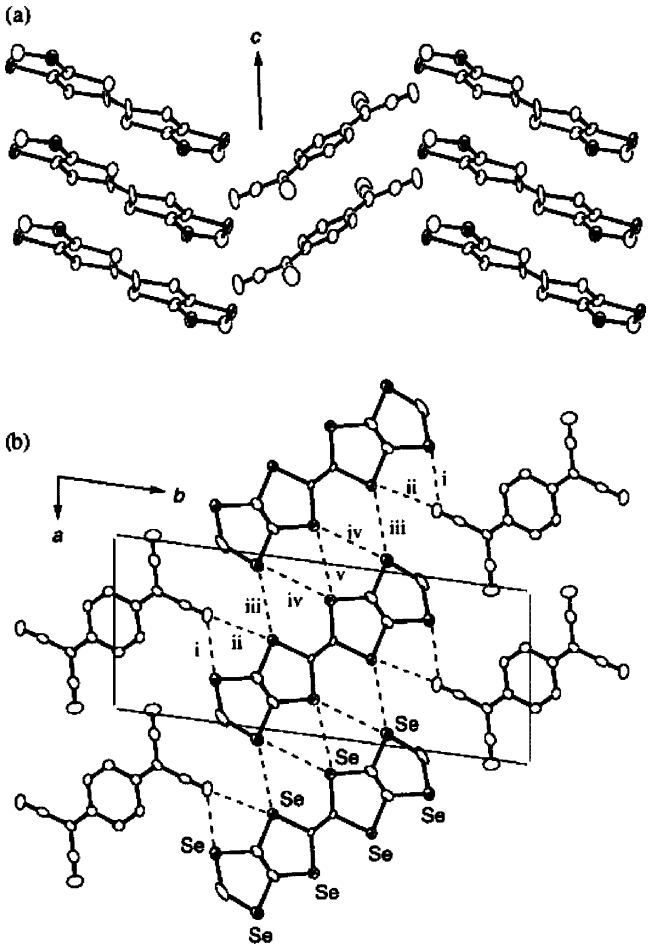

Figure 32. Crystal packing of BES-TSF:TCNQ: (a) view along the a axis and (b) view along the c axis showing Se−Se and Se···N contacts by dashed lines.

higher than the room-temperature value (Figure 33). The high conductivity of this complex is similar to that of other TSF derivatives HMTSF:TNAP (2200 ± 500 S cm^{-1})[69] and TTeF:TCNQ (2500 Ss cm^{-1}).[69] The high difference in conductivity between TCNQ

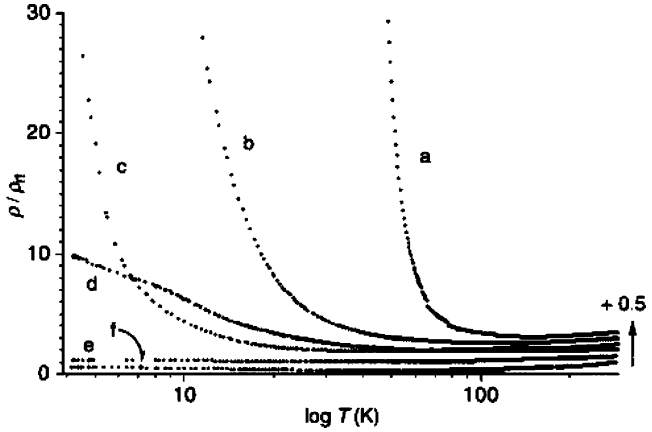

Figure 33. Normalized resistance vs temperature for the complexes and salts of BES-TTF: (a) ClO_4, (b) TCNQ, (c) AsF_6 and BES-TSF, (d) AsF_6, (e) ClO_4, and (f) TCNQ. The plots are displaced upward successively by $0.5\rho/\rho_{rt}$ from the bottom plot.

complexes of BES-TTF and BES-TSF is in line with the increase of conductivity of TCNQ complexes on going from TTF to TSF and TTeF.[70]

5.1.2.2. Radical−Ion Salts. Besides the charge-transfer complexes, Otsubo et al. also prepared several salts from BES-TTF and BES-TSF by electrocrystallization with simple monovalent anions such as ClO_4, PF_6, and AsF_6.[7,68] The only reported crystal structure is that of the $(BES\text{-}TTF)_2AsF_6$ salt, which is isostructural with the corresponding BET-TTF derivative, showing only small differences in the Se···S and Se···Se contacts.[52]

Interestingly, all salts display metallic character (Figure 33) as those salts derived from the BES-TSF donor are more stable metals since they do not have a clear metal−insulator transition but only a small localization at low temperature that can be attributed to some disorder in the crystal structure. The conductivity values (σ_{300} between 40 and 280 S cm^{-1}) are similar to those observed in the corresponding BET-TTF derivatives, indicating that, in contrast to the behavior observed in TCNQ complexes, substitution of S by Se does not lead to better transport properties in the derived salts.

5.2. From Dissymmetric Donors

Preparation of crystals of good quality for structural and physical characterization has been revealed to be harder for dissymmetrical donors than for BET-TTF. Nevertheless, good results have been obtained with ETT-TTF and ETEDT-TTF donors.

5.2.1. ETT-TTF Derivatives

The interest of this donor is that can be a good building block to prepare materials with interesting magnetic characteristics by combination with the $M(mnt)_2$ (M ≃ Au, Pt, Ni) counterions. In fact, the symmetric counterpart, DT-TTF donor, forms very interesting compounds by combination with $M(mnt)_2$ anions, i.e., spin-ladder behavior is found when M ≃ Au, Cu,[71] and interactions between delocalized electrons in the DT-TTF lattice and localized electrons in the anion are observed when the anions are paramagnetic $M(mnt)_2$ (M ≃ Ni, Pt).[72] The similarities of the electronic and structural properties of DT-TTF and ETT-TTF donors make the latter very promising for purposes of forming spin-ladder compounds by combination with the $[Au(mnt)_2]^-$ anion.

In fact, by electrocrystallization of the donor ETT-TTF with the tetrabutylammonium salt of the $[Au(mnt)_2]^-$ anion, the mixed-valence salt $(ETT\text{-}TTF)_2[Au(mnt)_2]$, which crystallizes in the monoclinic space group $P2_1/n$, isostructural with the $(DT\text{-}TTF)_2[Au(mnt)_2]$ salt, was obtained.[24] ETT-TTF molecules in the crystal are disordered with 50% of the molecules in one position and 50% in the position resulting from a rotation of 180° around the central C=C bond, although in contrast with the neutral ETT-TTF donor no disorder in the position of the external rings was found.

Molecules of both ETT-TTF and $[Au(mnt)_2]$ form segregated tilted stacks along the *b* axis in a herringbone pattern (Figure 34) with the ETT-TTF stacks arranged in pairs that are strongly connected through five short S···S contacts forming in that way a structural ladder. As in the case of the $(DT\text{-}TTF)_2[Au(mnt)_2]$ salt, the crystal structure of $(ETT\text{-}TTF)_2[Au(mnt)_2]$ is very similar to that of the donor component, the ETT-TTF (Figure 8),[13,24] and can be generated from this one by intercalating one column of anions every two columns of donors.

Electrical conductivity of $ETT\text{-}TTF_2[Au(mnt)_2]$ along the chain axis *b* is thermally activated with a room-temperature conductivity value of 3.6 S cm^{-1}. This behavior is consistent with the 1D ladder structure and a narrow band, similar to that observed in the isostructural $DT\text{-}TTF_2[Au(mnt)_2]$ salt which has a small bandwidth.[71a,73] The absence of a transition in $ETT\text{-}TTF_2[Au(mnt)_2]$ salt can be due to the formation of dimers already at room temperature. The quality of crystals of $ETT\text{-}TTF_2[Au(mnt)_2]$ was not good enough to perform X-ray scattering experiments, which can confirm this possibility.

Concerning the magnetic properties, ESR parameters of an oriented crystal of $ETT\text{-}TTF_2[Au(mnt)_2]$ salt are very similar to those found in the isostructural DT-TTF derivative, and the large susceptibility value at room temperature (20×10^{-4} emu/mol), which gave an effective magnetic moment corresponding to one spin per formula unit, is consistent with localization of electrons already at room temperature. This behavior is due to the strongly correlated electrons in the ETT-TTF chains, in agreement with transport properties. Nevertheless, the temperature dependence of the susceptibility does not follow the expected spin-ladder behavior with a gap in the low-temperature region.[73] In contrast, the susceptibility is more consistent with the presence of antiferromagnetic interactions in various directions which can be mediated by the diamagnetic anions. The absence of spin-ladder magnetic behavior should be attributed to the disorder existent in the crystal structure of $[ETT\text{-}TTF]_2[Au(mnt)_2]$, which prevents the long-range dimer formation necessary to have localized spin carrier units interacting in a ladder mode. This explanation is in agreement with the existence of a large Curie tail due to defects in the crystals (10% of $S = 1/2$ impurities).

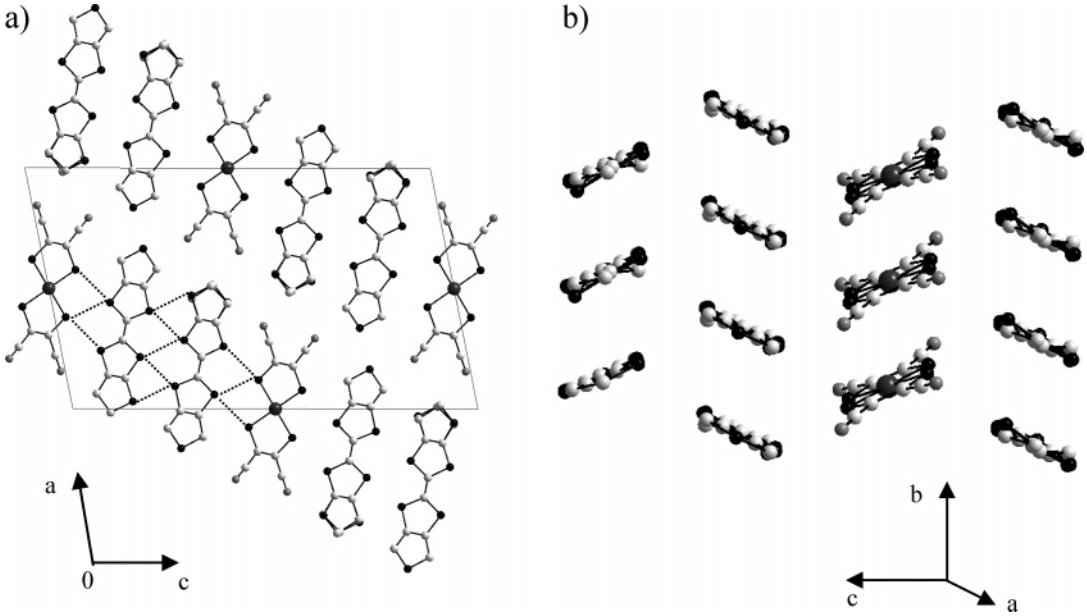

Figure 34. Crystal structure of ETT-TTF$_2$[Au(mnt)$_2$]; for clarity purposes, only one of the possible ETT-TTF molecules has been drawn. (a) View along the stacking axis *b*; dashed lines show S···S contacts shorter than 3.8 Å. (b) View parallel to the long molecular axes of ETT-TTF molecules.

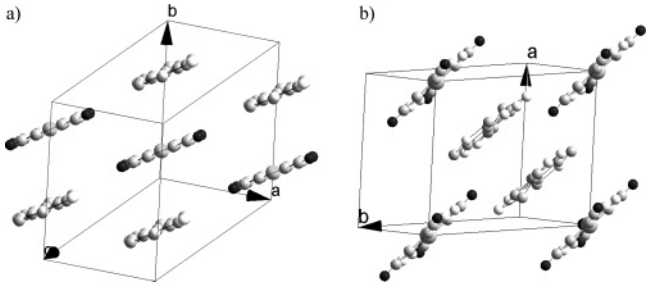

Figure 35. (a) View of the crystal packing of ETT-TTF-[Ni(mnt)$_2$]. (b) View of the crystal packing of (ETT-TTF)$_2$-[Pt(mnt)$_2$].

Another difference with the symmetric donor DT-TTF, which forms isostructural salts with all maleonitrilodithiolate complexes, M(mnt)$_2$ (M = Au, Ni, Pt, Cu), is that the dissymmetric donor ETT-TTF forms different salts with M(mnt)$_2$ (M = Pt, Ni). By electrocrystallization of ETT-TTF with the tetrabutylammonium salt of the bis-maleonitriledithiolate Pt(III) and Ni(III) complexes, only the salt (ETT-TTF)[Ni(mnt)$_2$] was obtained over platinum electrodes as a single crystal. On the other hand, single crystals of (ETT-TTF)$_2$[Pt(mnt)$_2$] (Pt(II)) were obtained by direct reaction of ETT-TTF and NBu$_4$-Pt(mnt)$_2^-$ solutions in CH$_3$CN using slow diffusion methodology. Both salts are completely ionic and crystallized forming mixed stacks (Figure 35).[74] The redox reaction between ETT-TTF and Pt(mnt)$_2^-$ that does not take place with the symmetric DT-TTF donor is possible since ETT-TTF shows better donor properties than DT-TTF (see Table 1).

5.2.2. ETEDT-TTF Derivatives

The disymmetric donor ETEDT-TTF, which can be considered as a combination of one-half BEDT-TTF and one-half BET-TTF, was supposed to form good materials similar to BEDT-TTF donor, which has to date provided the largest number of molecular superconductors· and forms the salt with the highest known T_c, 12.8 K.[75] Nevertheless, good crystals from ETEDT-TTF are by far not easy to obtain, and only with trihalides and octahedral monoanions XF$_6^-$ (X = P, Sb, As) some good materials were prepared.

By both electrochemical synthesis and direct chemical reactions the mixed-valence salts [ETEDT-TTF]-X$_{0.42}$ were obtained together with the corresponding completely ionic salts [ETEDT-TTF]X, where X = I$_3^-$ or I$_y$Br$_{3-y}^-$.[76] According to X-ray data, in the isostructural [ETEDT-TTF]X salts the donor radical cations are strongly dimerized with an interplane distance of 3.310−3.317 Å (Figure 36a) and the mixed-valence [ETEDT-TTF](I$_3$)$_{0.42}$ salt is formed by segregated radical cation and anion layers alternating along the *b* axis. The donor layers of [ETEDT-TTF](I$_3$)$_{0.42}$ have the typical θ-type packing (Figure 36b) and show semiconducting behavior with a high room-temperature conductivity of 24 S cm^{-1}. The large angle between the molecular planes of the donors in neighboring stacks precludes the possible metallic behavior of this salt, in accord with the work of Mori et al.[77] on the metallic vs semiconducting behavior of BEDT-TTF and BEDT-TSF θ-type salts. Both the band structure and Fermi surface of [ETEDT-TTF](I$_3$)$_{0.42}$ are the typical ones for θ-phases.[77]

Octahedral anions XF$_6$ (X = P, As, Sb) give rise to good quality crystals when combined with ETEDT-TTF donor.[78] With the three anions the donor forms isostructural salts with composition (ETEDT-TTF)$_2$XF$_6$ (X = P, As, Sb). Salts with different stoichiometry were also obtained by using different solvent but not in the same experiment, in contrast to the trend observed for BET-TTF (vide supra) or BEDT-TTF which tend to form different polymorphs.[1]

The three isostructural 2:1 salts crystallize in the triclinic P-1 space group, having two molecules per unit cell. The packing of molecules form head-to-tail zigzag stacks along the *b* axis with two kinds of

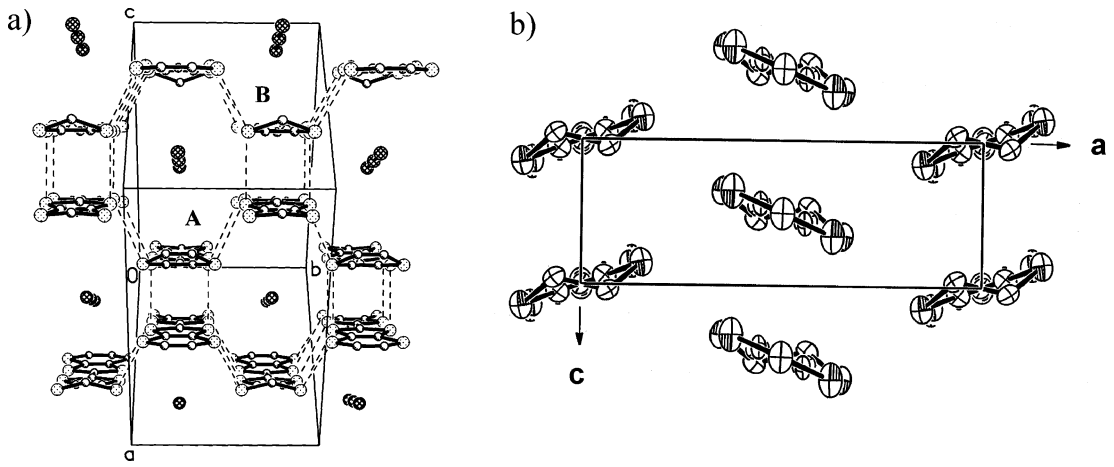

Figure 36. (a) View of the crystal packing of (ETEDT-TTF)I_3. (b) View of the donors layer in the crystal structure of (ETEDT-TTF)$(I_3)_{0.42}$ along the *b* direction.

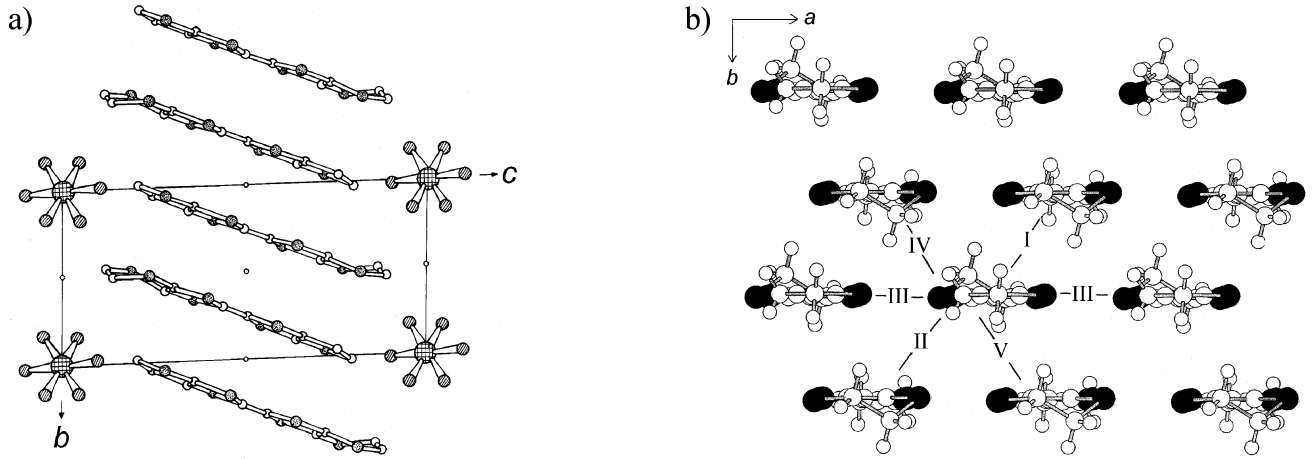

Figure 37. Crystal packing of (ETEDT-TTF)$_2SbF_6$. (a) View along the *a* axis showing the head-to-tail stacks of donors. (b) View of the donor layer showing the different HOMO−HOMO interactions.

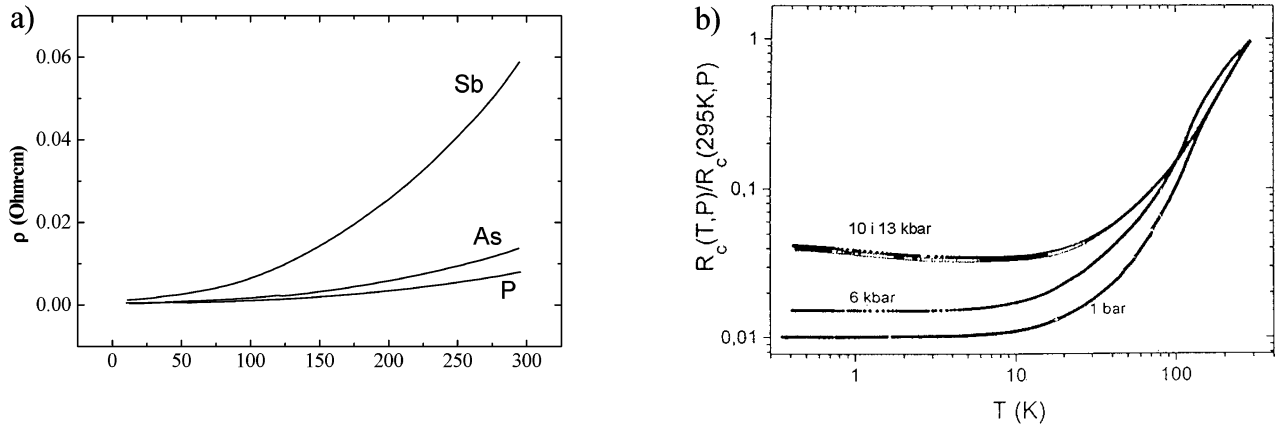

Figure 38. (a) Resistivity versus temperature of (ETEDT-TTF)$_2XF_6$ (X = P, As, Sb). (b) Temperature dependence of the normalized interplane resistance of the (ETEDT-TTF)$_2SbF_6$ crystal under different pressures.

intrastack molecular overlaps (Figure 37b). Short S···S distances along the stacking axis and between parallel stacks along the *a* axis as well as S···C and C···C contacts give rise to a 2D crystal packing reminiscent of the β-type packing observed in many BEDT-TTF derivatives and (BET-TTF)$_2XF_6$.[52]

Nevertheless, in these structures the HOMO−HOMO interactions are stronger in the interchain directions (III in Figure 37b) than in the intrachain ones.[79] There is disorder of the ethylene groups of the six-membered rings but not the typical disorder of the sulfur atom of the five-membered rings.

The three salts are stable metals down to 4 K (Figure 38a). (ETEDT-TTF)$_2SbF_6$ crystals were also measured down to 0.37 K; however, no evidence of a superconducting transition was observed. Moreover, with increasing pressure a small localization effect was observed which becomes more pronounced under high pressure (Figure 38b) in both interplane and inplane resistance.[79]

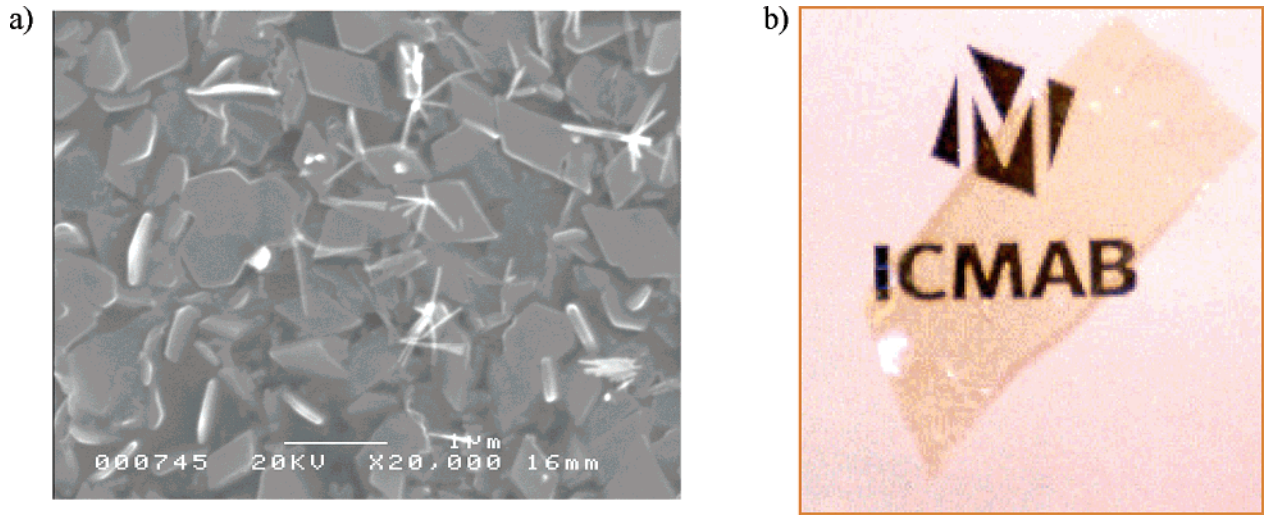

Figure 39. (a) SEM image of the surface layer of a BL film showing the network of θ-(BET-TTF)$_2$Br·3H$_2$O nanocrystals. (b) View through the metallic BL film.

6. Conducting Bilayered Films

To overcome the known technological limitations of single crystals of organic conductors (e.g., low processability, quantities), it is of great interest to prepare conducting bilayer composite films (BL films)[80] that consist of a polymeric matrix with a conducting surface layer formed by a nanocrystalline network of organic conductors. One great advantage of this method of preparation is that it results in a material that combines the unusual electronic properties of molecular metals (e.g., metallic conductivity, superconductivity) together with the favorable properties of a polymeric matrix (e.g., flexibility, transparency, low density). Furthermore, BL films can be produced with different sizes and shapes, which could be of technical interest. Therefore, they have clear advantages compared to the single crystals of molecular conductors concerning potential applications in a new generation of electronic devices.

From the above reviewed materials, θ-(BET-TTF)$_2$Br·3H$_2$O and θ-[ETEDT-TTF](X)$_{0.42}$ (X = I_3, I_yBr_{3-y}) with layered 2D structures, halogenated anions, and high room-temperature conductivities are appropriate as base components for the conducting layer of bilayer composite films (BL film).

Establishment of optimum conditions for the BL film preparation step, which implies reaction between BET-TTF and Br$_2$, allows one to generate a very transparent film containing a layer of highly oriented and well-connected θ-(BET-TTF)$_2$Br·3H$_2$O nanocrystals (Figure 39).[81]

The X-ray diffraction patterns indicate that the crystalline layers of the films are formed by θ-(BET-TTF)$_2$Br·3H$_2$O nanocrystals oriented with the crystallographic a*-axis perpendicular to the film surface, and consequently, the conducting plane of the crystals is parallel to it.

In Figure 39a the displayed SEM image of one film sample shows that an interlocked nanocrystalline network covers all the film surface, providing good contacts and, therefore, allowing good conductivity along the surface.

Both the UV−vis−NIR and ESR spectroscopies of the films reveal the same properties as the corresponding single crystals and confirm both the mixed-valence character and the high orientation of the crystals. The conductivity values at room temperature are extremely high compared with known BL films,[80] reaching values between 95 and 120 S cm^{-1}. In addition, these samples have metal-like transport properties down to He temperature (Figure 40), which in the layer of nanocrystals has the same properties as the single-crystal material, and the high conductivity observed is in accordance with the very high conductivity presented by the single crystals. It is important to emphasize that the metallic state of the films, as in the single crystals, is stable between 4 and 340 K, where an irreversible metal−insulator transition takes place.[82]

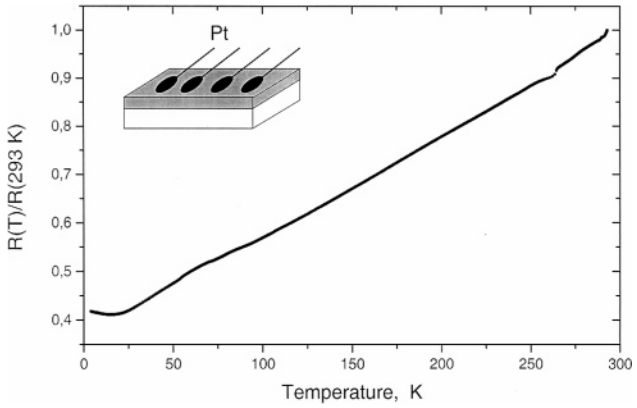

Figure 40. Normalized resistance of the conducting surface layer of θ-(BET-TTF)$_2$Br·3H$_2$O nanocrystals versus temperature. The inset shows the geometry of electrical contacts to the film sample.

Starting from the dissymmetric donor ETEDT-TTF and following the described methods for the preparation of BL films and using solutions of I$_2$ and IBr in CH_2Cl_2, two different sets of films were obtained.[76] These films have the same physical characteristics (flexibility, low density, and transparency) as the ones which have been previously reported even though their transparency is not as good as the one shown by the previous BET-TTF-based films.[80] SEM images also show a polycrystalline surface, and the diffraction pattern corresponds to the mixed-valence

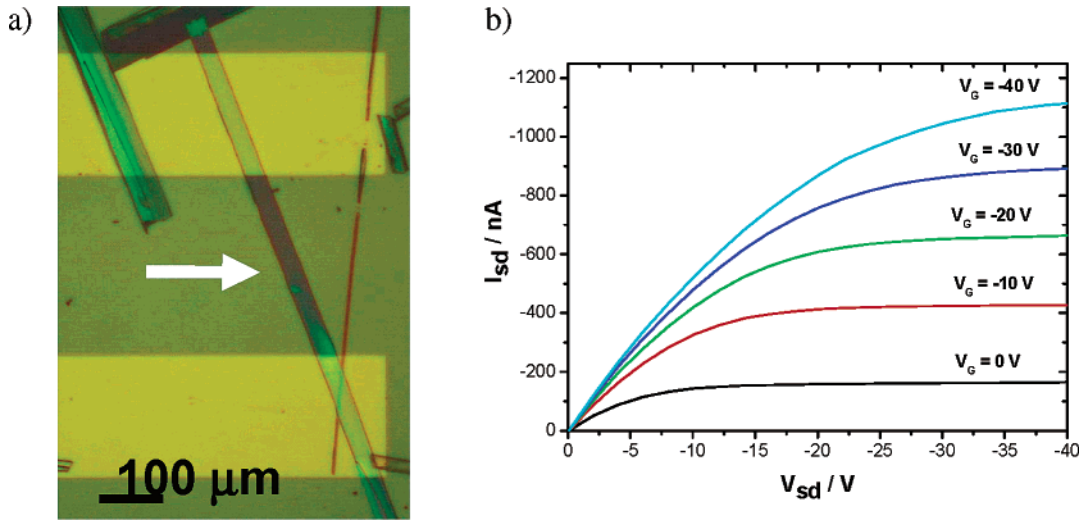

Figure 41. (a) DT-TTF crystal formed on microfabricated electrodes. (b) I_{SD} versus V_{SD} at constant V_G for a single-crystal OFET based on DT-TTF.

salts [ETEDT-TTF]$(I_3)_{0.43}$ and [ETEDT-TTF]$I_{1.20}Br_{0.08}$. Noteworthy, in most experiments producing good films, only the mixed-valence salts were obtained in contrast with the behavior of single crystals where completely ionic salts can be produced also.

It is worth mentioning that the ESR signal observed when the magnetic field was perpendicular to the film surface has the same ESR parameters as that of one of the directions of the single crystal, whereas when the field is parallel to the film the ESR parameters have an averaged value of the other two directions of the crystals. These results imply that oriented nanocrystals of the same θ phase have been formed on the film surface. The crystallographic c^*-axis of nanocrystals is perpendicular to the film surface, and consequently their conducting layers are parallel to it, although in a random orientation. This is in agreement with the SEM images in which all film samples contain oriented crystals with nanoscopic dimensions (200−300 nm) which have their largest face (ab plane) parallel to the film surface.

The σ_{293K} values of the films containing [ETEDT-TTF]$(I_3)_{0.43}$ and [ETEDT-TTF]$I_{1.20}Br_{0.08}$ were 0.25 and 2.5 S cm^{-1}, respectively, which is a notable conductivity for this kind of materials. The temperature dependence of the resistance of the BL films was measured down to 125 K, exhibiting the same semiconducting behavior as it was seen for the mixed-valence salt with iodine. Thus, the transport properties of the ETEDT-TTF family of conducting organic salts have been successfully moved to polymeric composite BL films.

Undoubtedly success in the preparation of BL films with physical properties of crystalline organic conductors is a step forward in the search for potential applications in the field of molecular electronics.

7. Organic Field-Effect Transistors Based on Single Crystals of Tetrathiafulvalene Derivatives

Organic field effect transistors (OFETs) have attracted a great deal of interest over the past few years in electronics due to their unique processing characteristics and improved electronic mobility.[83] To progress in the field of molecular electronics toward device applications, it is also very important to search for new molecules that are able to act as organic semiconductors and to develop easy methods to grow single crystals or films.

Clear observation of field effect hole mobility in single crystals of a TTF derivative with thiophene substituents was reported very recently, the organic semiconductor dithiophene-tetrathiafulvalene (DT-TTF) grown by drop casting, a very simple method. Due to the high solubility and processability of DT-TTF, this device (Figure 41a), in contrast to previously reported single-crystal devices, in which the crystals are grown from the vapor phase in long and complex experiments, was prepared using a simple room-temperature drop casting technique.[84]

The electrical measurements performed on the DT-TTF crystals are typical of a p-type semiconductor; as a more negative VG is applied, more holes are induced in the semiconductor and the conductivity increases (Figure 41b). The maximum mobility achieved was of 1.4 cm^2/Vs, which is the highest mobility reported for an organic semiconductor which is not based on pentacene and is on the order of that of amorphous silicon that is widely used in solar cells and flat screen displays.

An even more recent work[14] shows that the isostructural dissymmetric donor ETT-TTF also is a good semiconductor to form OFETs. Nevertheless, due to the disordered structure of this donor (see section 3.1.2) the highest mobilities achieved on a single crystal are 1 order of magnitude lower. With the TTF derivatives BET-TTF and ETEDT-TTF, which have completely different crystal packing (see sections 3.1.1 and 3.1.2), the mobilities are also high but lower than the previous ones that have a herringbone-type packing in their crystal structure. A trend in mobilities through the different crystal structures is observed which is further strongly corroborated by calculations of both the molecular reorganization energies and the maximum intermolecular transfer integrals.[85] Among the structures

studied, the herringbone crystal structure of DT-TTF, ETT-TTF, and TTDM-TTF is most suitable for preparing OFETs. The devices of this group exhibit the highest mobilities found for solution-processed materials and are also among the highest reported for OFETs.

The outstanding device performance and the fact that TTF derivatives can be easily processed opens new perspectives in the field of OFETs. In fact, this result responds to the current need to find materials which show high mobilities, are solution-processed, and, therefore, are suitable for low-cost electronics.

8. Concluding Remarks

Both the electronic and supramolecular characteristics of BET-TTF and most of the related donors discussed in this review are appropriate to prepare molecular functional materials with very interesting properties even though the lack of complete symmetry of these donors induces in most materials localization effects at low temperature.

BET-TTF forms crystalline radical−ion salts with simple monovalent anions of different geometries where the donor forms typical layered donor−anion structures. Some of the salts with 1:1 stoichiometry maintain the same parallel packing as the neutral BET-TTF donor, whereas the crystal structures of most of the salts with 2:1 stoichiometry are very similar and resemble the β-type salts of BEDT-TTF. In the salts with a 3:2 stoichiometry, the intercalation mode of the anion promotes an α-type crystal packing. On the other hand, with less common anions having planar shape or higher charge, dimers of BET-TTF are formed showing different packing with each anion.

A characteristic of the BET-TTF-based functional materials is that although salts with different composition can grow in the same experiment, no polymorphs of a given salt have so far been obtained, which differentiate BET-TTF from the BEDT-TTF donor. Due to the greater rigidity of the external five-membered rings with respect to the six-membered ring of BEDT-TTF, in BET-TTF salts there is no disorder associated with the ethylene groups but a disorder is observed due to the position of the external sulfur atoms and cis and trans isomers can be present at the same time in a salt. Despite this characteristic, most of the mixed-valence salts of BET-TTF are metallic although they undergo broad M−I transitions at low temperature. The origin of the transitions can be attributed to localization of the electrons due to the disorder shown by the BET-TTF donors in the crystals. This point is in accordance with the stable metallic character of the salts (BET-TTF)$_2$X·3H$_2$O (X = Br, Cl) in which only completely ordered *trans*-BET-TTF donors are found in the cationic layer.

From the few materials prepared from the analogous Se-containing donors as well as from the dissymmetric donors, similar conclusions can be drawn since various compounds showing very good metallic properties have been developed.

With halogenated derivatives of both BET-TTF and ETEDT-TTF the good properties of the single crystals have been successfully transferred to polymeric films, resulting in transparent flexible materials with conducting properties which open the way for application of the charge-transfer salts.

Finally, not only have charged materials been useful for applications in molecular electronics, but also neutral TTF derivatives with planar molecules in the crystals, especially those with thiophene substituents, have proved to be good semiconductors for the preparation of organic field effect transistors (OFETS). The facile processing and easy chemical modification of TTF derivatives opens a very promising way for TTF derivatives in the molecular electronics field.

9. Acknowledgments

First, I wish to particularly thank Dwaine O. Cowan for introducing me to the fascinating world of molecular conducting materials. A lot of students, postdoctoral fellows, and co-workers, which appear in the references, are responsible for the work presented, and I wish to acknowledge them for making possible achievement of the results and the helpful discussions maintained. Special thanks to Professor J. Veciana, Dr. M. Mas-Torrent, Dr. E. Ribera, Dr. J. Tarrés, Dr. X. Ribas, Professor E. Canadell, Professor V. Laukhin, Dr. J. Vidal-Gancedo, Dr. E. Laukhina, A. Pérez-Benítez, Dr. N. Santaló, Professor J. Novoa, Dr. M-C. Rovira, Professor E. Coronado, Dr. C. Gómez, Professor M. Almeida, Professor R. T. Henriques, Dr. V. Gama, Dr. Dulce Belo, Dr. K. Wurst, Prof. R. Shibaeva, Dr. S. Kasanov, and Dr. P. Hadley. This work was supported by grants from DGI Spain (Projects BQU2003-00760), DGR Catalonia (Project 2001SGR00362), Catalan Network CeRMAE, and ICCT-CSIC bilateral agreement and benefited also from COST D14.

10. References

(1) (a) Cowan, D. O. In *New Aspects of Organic Chemistry*; Yoshida, Z., Shiba, T., Ohshiro, Y., Eds.; Kodama: Tokyo, 1989. (b) Saito, G.; Kagoshima, S. *The Physics and Chemistry of Organic Superconductors*; Springer: Berlin, 1990. (c) Williams, J. M.; Ferraro, J. R.; Thorn, R. J.; Carlson, K. D.; Geiser, U.; Wang, H. H.; Kini, A. M.; Whangbo, M.-H. *Organic Superconductors (Including Fullerenes) Synthesis, Structure, Properties, and Theory*; Prentice Hall: Englewood Cliffs, NJ, 1992. (d) Farges, J.-P. *Organic Conductors; Fundamentals and Applications*; Marcel-Dekker Inc.: New York, 1994. (e) Ishiguro, T.; Yamaji, K.; Saito, G. *Organic Superconductors*; Springer-Verlag: New York, 1998. (f) Veciana, J.; Rovira C.; Amabilino, D. B. *Supramolecular Engineering of Synthetic Metallic Materials: Conductors and Magnets*; Kluwer Academic Publishers: Dordrecht, 1999.

(2) (a) Narita, M.; Pittmam, C. U. *Synthesis* **1976**, 489. (b) Krief, A. *Tetrahedron* **1986**, *42*, 1209. (c) Bryce, M. R. *Chem. Soc. Rev.* **1991**, *20*, 355. (d) Garín, J. *Adv. Heterocycl. Chem.* **1995**, *62*, 249. (e) Schukat, G.; Fanghänel, E. *Sulfur Rep.* **1996**, *18*, 1. (f) Nielsen, M. B.; Lomholt, C.; Becher, J. *Chem. Soc. Rev.* **2000**, *29*, 153.

(3) (a) Novoa, J. J.; Rovira, M. C.; Rovira, C.; Veciana, J.; Tarrés, J. *Adv. Mater.* **1995**, *7*, 233. (b) Rovira, C.; Novoa, J. J. *Chem. Eur. J.* **1999**, *5*, 3689

(4) Engler, E. M.; Patel, V. V.; Andersen, J. R.; Shumaker, R. R.; Fukushima, A. A. *J. Am. Chem. Soc.* **1978**, *100*, 3769.

(5) Spencer, H. K.; Cava., M. P.; Yamagishi, F. G.; Garito, A. F. *J. Org. Chem.* **1976**, *41*, 730.

(6) Rovira, C.; Veciana, J.; Santaló, N.; Tarrés, J.; Cirujeda, J.; Molins, E.; Llorca, J.; Espinosa, E. *J. Org. Chem.* **1994**, *59*, 3307.

(7) (a) Jigami, T.; Takimiya, K.; Aso, Y.; Otsubo, T. *Chem. Lett.* **1997**, 1091. (b) Jigami, T.; Takimiya, K.; Otsubo, T.; Aso, Y. *J. Org. Chem.* **1998**, *63*, 8865. (c) Otsubo, T.; Takimiya, K.; Aso, Y. *Phosphorous Sulfur* **2001**, *171*, 231.

(8) Pérez-Benítez, A.; Tarrés, J.; Ribera, E.; Veciana, J.; Rovira, C. *Synthesis* **1999**, 577.
(9) Belo, D.; Alves, H.; Lopes, E. B.; Duarte, M.-T.; henriques, R. T.; Almeida, M.; Pérez-Benítez, A.; Rovira, C.; Veciana, J. *Chem. Eur. J.* **2001**, *7*, 511.
(10) (a) Yamashita, Y.; Tomura, M.; Tanaka, S. *J. Chem. Soc., Perkin Trans.* **1990**, *1*, 3358 (b) Larsen, J.; Lenoir, C. *Synthesis* **1989**, 134.
(11) Rovira, C. Unpublished results.
(12) Ribera, E.; Veciana, J.; Molins, E.; Mata, I.; Wurst, K.; Rovira, C. *Eur. J. Org. Chem* **2000**, 2867−2875.
(13) Tarrés, J. Doctoral Thesis, Barcelona University, 1997.
(14) Mas-Torrent, M.; Hadley, P.; Bromley, S. T.; Ribas, X.; Tarrés, J.; Mas, M.; Molins, E.; Veciana, J.; Rovira, C. *J. Am. Chem. Soc.* **2004**, *126*, 8546.
(15) Souizi, A.; Robert, A.; Batail, P.; Ouahab, L. *J. Org. Chem.* **1987**, *52*, 1610.
(16) (a) Kobayashi, H.; Kobayashi, A.; Sasaki, Y.; Saito, G.; Inokuchi, H. *Bull. Chem. Soc. Jpn.* **1986**, *59*, 301. (b) Novoa, J. J.; Rovira, M. C.; Rovira, C.; Veciana, J.; Tarrés, J. *Adv. Mater.* **1995**, *7*, 233.
(17) Kato, R.; Kobayashi, H.; Kobayashi, A.; Sasaki, Y. *Chem. Lett.* **1985**, 1231.
(18) Saito, K.; Ishikawa, Y.; Kikuchi, K.; Ikemoto, I. *Acta Crystallogr.* **1989**, *C45*, 1403.
(19) Kobayashi, H.; Kobayashi, A.; Sasaki, Y.; Saito, G.; Inokuchi, H. *Bull. Chem. Soc. Jpn.* **1986**, *59*, 301.
(20) Rovira, M. C.; Novoa, J. J.; Tarrés, J.; Rovira, C.; Veciana, J.; Yang, S.; Cowan, D. O.; Canadell, E. *Adv. Mater.* **1995**, *7*, 1023.
(21) Williams, J. M.; Wang, H.-H.; Emge, T. J.; Geiser, U.; Beno, M. A.; Leung, P. C. W.; Carlson, K. D.; Thorn, R. J.; Schultz, A. J.; Whangbo, M.-H. *Prog. Inorg. Chem.* **1987**, *35*, 51.
(22) The crystal structure of BES-TSF was obtained from Cambridge Database (reference name HOBMIU).
(23) Rovira, M. C. Doctoral Thesis, Universitat de Barcelona, 1995.
(24) Rovira, C.; et al. Submitted for publication.
(25) Saito, Y.; Ishikawa, K.; Kikuchi, I.; Ikemoto, K.; Kobayashi, *Acta Crystallogr.* **1989**, *C45*, 1403−1406.
(26) Garreau, B.; Mountauzon, D. D.; Cassoux, P.; Legros, J. P.; Fabre, J.-M.; Saoud, K.; Chakroune, S. *New J. Chem.* **1995**, *19*, 161−71.
(27) (a) Cooper, W. F.; Kenny, N. C.; Eduards, J. W.; Nagel, A.; Wudl, F.; Coppens, P. *J. Chem. Soc. D* **1971**, *16*, 889. (b) Cooper, W. F.; Edwards, J. W.; Wudl, F.; Coppens, P. *Cryst. Struct. Commun.* **1974**, *3*, 23.
(28) Ellern, A.; Bernstein, J.; Becker, J. Y.; Zamir, S.; Shahal, L. *Chem. Mater.* **1994**, *6*, 1378.
(29) Llacay, J.; Mata, I.; Molins, E.; Veciana, J.; Rovira, C. *Adv. Mater.* **1998**, *3*, 330.
(30) Lichtenberger, D. L.; Johnston, R. L.; Hinkelmann, K.; Suzuki, T.; Wudl, F. *J. Am. Chem. Soc.* **1990**, *112*, 3302.
(31) Schukat, G.; Richter, A. M.; Fanghänel, E. *Sulfur Rep.* **1987**, *7*, 155.
(32) Santaló, N. Doctoral Thesis, Universitat de Barcelona, 1991.
(33) Santaló, N.; Veciana, J.; Rovira, C.; Molins, E.; Miravitlles, C.; Claret, J. *Synth. Met.* **1991**, *42*, 2205.
(34) Chapell, J. S.; Bloch, A. N.; Bryden, W. A.; Maxfield, M.; Pooehler, T. O.; Cowan, D. O. *J. Am. Chem. Soc*, **1981**, *103*, 2442.
(35) (a) Santaló, N.; Tarrés, J.; Veciana, J.; Rovira, C.; Molins, E.; Cowan, D. O.; Delhaes, P.; Canadell, E. *Synth. Met.* **1993**, *56*, 2050. (b) Rovira, C.; Tarrés, J.; Llorca, J.; Molins, E.; Veciana, J.; Yang, S.; Cowan, D. O.; Garrigou-Lagrange, C.; Amiell, J.; Delhaes, P.; Canadell, E.; Pouget, J. P. *Phys. Rev. B* **1995**, *52*, 8747.
(36) (a) Llacay, J.; Tarrés, J.; Veciana, J.; Rovira, C. *Synth. Met.* **1995**, *70*, 1453. (b) Llacay, J.; Tarrés, J.; Rovira, C.; Veciana, J.; Mas, M.; Molins, E. *J. Phys. Chem. Solids* **1997**, *58*, 1675.
(37) (a) Izouka, A.; Tachikawa, T.; Sugawara, T.; Suzuki, M.; Konno, M.; Saito, Y.; Shinohara, H. *J. Chem. Soc., Chem. Commun.* **1992**, 1472. (b) Saito, G.; Teramoto, T.; Otsuka, A.; Sugita, Y.; Ban, T.; Kusunoki, M.; Sakaguchi, K. *Synth. Met.* **1994**, *64*, 359.
(38) Allemand, P. M.; Srdanov, G.; Koch, A.; Khemani, K.; Wudl, F.; Rubin, Y.; Diederich, F.; Alvarez, M. M.; Anz, S. J.; Whetten, R. L. *J. Am. Chem. Soc.* **1991**, *113*, 2780.
(39) Laukhina, E.; Vidal-Gancedo, J.; Laukhin, V.; Veciana, J.; Chuev, I.; Tkacheva, V.; Wurst, K.; Rovira, C. *J. Am. Chem. Soc.* **2003**, *125*, 3948.
(40) Rovira, C.; Veciana, J.; Tarrés, J.; Molins, E.; Mas, M.; Cowan, D. O.; Yang, S. *Synth. Met.* **1995**, *70*, 883.
(41) Bozio, R.; Zanon, I.; Girlando, A.; Pecile, C. *J. Chem. Phys.* **1979,** *71*, 2282.
(42) Rovira, C.; Tarrés, J.; Ribera, E.; Veciana, J.; Canadell, E.; Molins, E.; Mas, M.; Laukhin, V.; Doublet, M.-L.; Cowan, D. O.; Yang, S. *Synth. Met.* **1997**, *86*, 2145.
(43) Boubekeur, K.; Lenoir, C.; Batail, P.; Carlier, R.; Tallec, A.; Le Paillard, M.-P.; Lorcy, D.; Robert, A. *Angew. Chem., Int. Ed. Engl.* **1994**, *33*, 1379.
(44) Laukhin, V. Unpublished results.
(45) Pérez-Benítez, A.; Rovira, C.; Veciana, J.; Vidal-Gancedo, J.; Laukhin, V. N.; Zorina, L. V.; Kasanov, S. S.; Narymbetov, B. Zh.; Shibaeva, R. P. *Synth. Met.* **1999**, *102*, 1707.
(46) Khasanov, S. S.; Pérez-Benítez, A.; Narymbetov, L.; Zorina, L. V.; Shibaeva, R. P.; Singleton, J.; Klehe, A.-K.; Laukhin, V. N.; Vidal-Gancedo, J.; Veciana, J.; Canadell, E.; Rovira, C. *J. Mater. Chem.* **2002**, *12*, 432.
(47) (a) Parkin, S. S.; Engler, E. M.; Schumaker, R. R.; Lagier, R.; Lee, V. Y.; Voiron, J.; Carneiro, K.; Scott, J. C.; Green, R. L. *J. Phys.* **1983**, *44*, C3−791; (b) Carneiro, K.; Scott, J. C.; Engler, E. M. *Solid State Commun.* **1984**, *50*, 477. (c) Parkin, S. S. P.; Engler, E. M.; Lee, V. Y.; Schumaker, R. R. *Mol. Cryst. Liq. Cryst.* **1985**, *119*, 375. (d) Kobayashi, H.; Kobayashi, A.; Sasaki, Y.; Saito, G.; Inokuchi, H.; *Chem. Lett.* **1984**, 183. (e) Schumaker, R. R.; Lee, V. Y.; Engler, E. M. *J. Phys.* **1983**, *44*, C3−1139.
(48) Parkin, S. S. P.; Engler, E. M.; Schumaker, R. R.; Lagier, R.; Lee, V. Y.; Scott, J. C.; Green, R. L. *Phys. Rev. Lett.* **1983**, *50*, 270.
(49) Coronado, E.; Falvello, L. R.; Galán-Mascarós, J. R.; Giménez-Saiz, C.; Gómez-García, C. J.; Laukhin, V. N.; Pérez-Benítez, A.; Rovira, C.; Veciana, J. *Adv. Mater.* **1997**, *9*, 984.
(50) Kobayashi, H.; Tomita, H.; Naito, T.; Kobayashi, A.; Sakai, F.; Watanabe, T.; Cassoux, P. *J. Am. Chem. Soc.* **1996**, *118*, 368.
(51) (a) Uji, S.; Kobayashi, H.; Balicas, L.; Brooks, J. *Adv. Mater.* **2002**, *14*, 243. (b) Uji, S.; Shinagawa, H.; Terashima, T.; Yakabe, T.; Terai, Y.; Tokumoto, M.; Kobayashi, A.; Tanaka, H.; Kobayashi, H. *Nature* **2001**, *410*, 908.
(52) Tarrés, J.; Santaló, N.; Mas, M.; Molins, E.; Veciana, J.; Rovira, C.; Yang, S.; Lee, H.; Cowan, D. O.; Doublet, M.-L. Canadell E. *Chem. Mater.* **1995**, *7*, 1558.
(53) Ribera, E.; Rovira, C.; Veciana, J.; Laukhin, V.; Canadell, E.; Vidal-Gancedo, J.; Molins, E. *Synth. Met.* **1997**, *86*, 1993.
(54) Ribera, E. Doctoral Thesis, Universitat Autònoma de Barcelona, 1999.
(55) Carducci, M. D.; Pressprich, M. R.; Coppens, P. *J. Am. Chem. Soc.* **1997**, *119*, 2669.
(56) (a) Graham, A. W.; Kurmoo, M.; Day, P. *J. Chem. Soc., Chem. Commun.* **1995**, 2061. (b) Kurmoo, M.; Graham, A. W.; Day, P.; Coles, S. J.; Hursthouse, M. B.; Caufield, J. L.; Singleton, J.; Pratt, F. L.; Hayes, W.; Ducasse, L.; Guionneau, *J. Am. Chem. Soc.* **1995**, *117*, 12209. (c) Coronado, E.; Galán-Mascarós, J. R.; Goméz-García, C. J.; Laukhin, V. *Nature* **2000**, *408*, 447.
(57) (a) Yu, H.; Zhu, D. *Physica C* **1997**, *282−287*, 1893. (b) Gener, M.; Canadell, E.; Khasanov, S. S.; Zorina, L. V.; Shibaeva, R. P.; Kushch, L. A.; Yagubskii, E. B. *Solid State Commun* **1999**, *111*, 329. (c) Kushch, L.; Buravov, L.; Tkacheva, V.; Yagubskii, E.; Zorina, L.; Khasanov, S.; Shibaeva, R. *Synth. Met.* **1999**, *102*, 1646. (d) Clemente-León, M.; Coronado, E.; Galán-Mascarós, J. R.; Giménez-Saiz, C.; Gómez-García, C. J.; Fabre, J. M. *Synth. Met.* **1999**, *103*, 2279. (e) Clemente-León, M.; Coronado, E.; Galán-Mascarós, J. R.; Gómez-García, C. J.; Canadell, E. *Inorg. Chem.* **2000**, *39*, 5394.
(58) Clemente-León, M.; Coronado, E.; Galán-Mascarós, J. R.; Giménez-Saiz, C.; Gómez-García, C. J.; Ribera, E.; Vidal-Gancedo, J.; Rovira, C. Canadell, E.; Laukhin, V. *Inorg. Chem.* **2001**, *40*, 3526.
(59) Clemente-León, M. Ph. Doctoral Thesis, University de Valencia (Spain), 1999.
(60) (a) Tarrés, J.; Veciana, J.; Rovira, C. *Synth. Met.* **1995**, *70*, 1167. (b) Laukhina, E.; Ribera, E.; Vidal-Gancedo, J.; Khasanov, S.; Zorina, L.; Shibaeva, R.; Canadell, E.; Laukhin, V.; Honold, M.; Nam, M.-S.; Singleton, J.; Veciana, J.; Rovira, C. *Adv. Mater.* **2000**, *12*, 54.
(61) (a) Kobayashi, H.; Kato, R.; Kobayashi, A.; Nishio, I.; Kajita, K.; Sasaki, W. *Chem. Lett.* **1986**, 789. (b) Shibaeva, R. P.; Khasanov, S. S.; Narymbetov, L.; Zorina, L. V.; Rosemberg, L. P.; Bazhenov, A. V.; Kushch, N. D.; Yagubskii, E. B.; Rovira, C.; Canadell, E. *J. Mater. Chem.* **1998**, *8*, 1151.
(62) Tarrés, J.; Mas, M.; Molins, E.; Veciana, J.; Rovira, C.; Morgado, J.; Henriques, R. T.; Almeida, M. *J. Mater. Chem.* **1995,** *5*, 1658.
(63) Rovira, C.; LeMoustarder, S.; Belo, D.; Veciana, J.; Almeida, M.; Gama, V.; Duarte, M. T. *Synth. Met.* **2001**, *120*, 717.
(64) Matos, M. J.; Santos, I.; Henriques, R. T.; Duarte, M. T. *Synth. Met.* **1991**, *41−43*, 2155.
(65) Shibaeva, R. P.; Kaminski, V. F.; Simonov, M. A.; Yagubskii, E. B.; Kostioshenko, E. E. *Kristallografia* **1995**, *30*, 488.
(66) Coronado, E.; Gómez-García, C. J. *Chem. Rev.* **1998**, *98*, 273.
(67) Coronado, E.; Galán-Mascarós, J. R.; Giménez-Saiz, C.; Gómez-García, C. J.; Rovira, C.; Tarrés, J.; Triki, S.; Veciana, J. *J. Mater. Chem.* **1998**, *8*, 313.
(68) Jigami, T.; Takimiya, K.; Aso, Y.; Otsubo, T. *Synth. Met.* **1999**, *102*, 1714.
(69) Bechgaard, K.; Jacobsen, C. S.; Andersen, N. H. *Solid State Commun.* **1978**, *25*, 1561.
(70) Cowan D. O.; Mays, M. D.; Kistenmacher, T. J.; Poehler, T. O.; Beno, M. A.; Kini, M. A.; Williams, J. M.; Kwik, Y. K.; Carlson, K. D.; Xiao, L.; Novoa, J. J.; Whangbo, M. H. *Mol. Cryst. Liq. Cryst.* **1990**, *181*, 43.
(71) (a) Rovira, C.; Veciana, J.; Ribera, E.; Tarres, J.; Candell, E.; Rousseau, R.; Mas, M.; Molins, E.; Almeida, M.; Henriques, R.

T.; Morgado, J.; Schoeffel, J.-P.; Pouget, J.-P. *Angew. Chem., Int. Ed. Engl.* **1997**, *36*, 2324. (b) Wesolowski, R.; Haraldsen, J. T.; Musfeldt, J. L.; Barnes, T.; Mas-Torrent, M.; Rovira, C.; Henriques, T.; Almeida, M. *Phys. Rev. B* **2003**, *68*, 134405. (c) Dias, J. C.; Lopes, E. B.; Santos, I. C.; Duarte, M. T.; Henriques, R. T.; Almeida, M.; Ribas, X.; Rovira, C.; Veciana, J.; Foury-Leylekian, P.; Pouget, J.-P.; Auban-Senzier, P.; Jérome, D. *J. Phys. IV Fr.* **2004**, *112*, 497.

(72) Ribera, E.; Rovira, C.; Veciana, J.; Tarrés, J.; Canadell, E.; Rousseau, R.; Molins, E.; Mas, M.; Schoeffel, J.-P.; Pouget, J.-P.; Morgado, J.; Henriques, R. T.; Almeida, M. *Chem. Eur. J.* **1999**, *5*, 2025.

(73) (a) Dagotto, E.; Rice, T. M.; *Science* **1996**, *271*, 618 (b) Troyer, M.; Tsunetsugu, D.; Würtz, D. *Phys. Rev. B* **1994**, *50*, 13315.

(74) Rovira, C.; Pérez-Benítez, A.; Alves, H.; Veciana, J.; Almeida, M.; Gama, V. *Synth. Met.* **2003**, *133*−*134*, 523.

(75) Williams, J. M.; Kini, A. M.; Wang, H. H.; Carlson, K. D.; Geiser, U.; Montgomery, L. K.; Pyrca, G. J.; Watkins, D. M.; Kommers, J. M.; Boryschuk, S. J.; Crouch, A. V. S.; Kwok, W. K.; Schirber, J. E.; Overmyer, D. L.; Jung, D.; Whangbo, M.-H. *Inorg. Chem.* **1990**, *29*, 3262.

(76) Mas-Torrent, M.; Ribera, E.; Tkacheva, V.; Mata, I.; Molins, E.; Vidal-Gancedo, J.; Khasanov, S.; Zorina, L.; Shibaeva, R.; Wojciechowski, R.; Ulanski, J.; Wurst, K.; Veciana, J.; Laukhin, V.; Canadell, E.; Laukhina E.; Rovira, C. *Chem. Mater.* **2002**, *14*, 3295.

(77) (a) Mori, T.; Mori, H.; Tanaka, S. *Bull. Chem. Soc. Jpn.* **1999**, *72*, 179. (b) Mori, H.; Sakurai, N.; Tanaka, S.; Moriyama, H.; Mori, T.; Kobayashi, H.; Kobayashi, A. *Chem. Mater.* **2000**, *12*, 2984.

(78) Rovira, C.; Ribera, E.; Veciana, J.; Laukhin, V. N.; Molins, E.; Mata, I.; Kasanov, S. S.; Zorina, L. V.; Narymbetov, B. Zh.; Shibaeva, R. P.; Wurst, K. *Synth. Met.* **1999**, *103*, 2224.

(79) Laukhin, V. N.; Ribera, E.; Rovira, C.; Veciana, J.; Gener, M.; Canadell, E.; Togonidze, T.; Kasanov, S. S.; Shibaeva, R. P.; Biberacher, W.; Andres, K.; Kartsovnik. *Synth. Met.* **1999**, *103*, 1772.

(80) (a) Laukhina, E. E.; Merzhanov, V. A.; Pesotskii, S. I.; Khomenko, A. G.; Yagubskii, E. B.; Ulanski, J.; Kryszewski, M.; Jeszka, J. K. *Synth. Met.* **1995**, *70*, 797. (b) Laukhina, E. E.; Ulanski, J.; Khomenko, A. G.; Pesotskii, S. I.; Tkachev, V.; Atovmyan, L.; Yagubskii, E. B.; Rovira, C.; Veciana, J.; Vidal-Gancedo, J.; Laukhin, V. *J. Phys. I Fr.* **1997,** *7*, 1665. (c) Horiuchi, S.; Yamochi, H.; Saito, G.; Jeszka, J. K.; Tracz, A.; Sroczyñska, A.; Ulanski, J. *Mol. Cryst. Liq. Cryst.* **1997**, *296*, 365. (d) Laukhina, E.; Tkacheva, V.; Shibaeva, R.; Khasanov, S.; Rovira, C.; Veciana, J.; Vidal-Gancedo, J.; Tracz, A.; Jeszka, J. K.; Sroczynska, A.; Wojciechowski, R.; Ulanski, J.; Laukhin, V. *Synth. Met.* **1999**, *102*, 1785.

(81) Mas-Torrent, M.; Laukhina, E.; Rovira, C.; Veciana, J.; Tkacheva, V.; Zorina, L.; Khasanov, S. *Adv. Funct. Mater.* **2001**, *11*, *4*, 299.

(82) Laukhina, E.; Pérez-Benítez, A.; Mas-Torrent, M.; Ribera, E.; Vidal-Gancedo, J.; Veciana, J.; Rovira, C.; Laukhin, V. In *Molecular Low Dimensional and Nanostructured Materials for Advanced Applications*; Graja, A., et al., Eds.; pp 277−284.

(83) Dimitrakopoulos, C. D.; Malenfant, P. R. L. *Adv. Mater.* **2002**, *14*, 99.

(84) Mas-Torrent, M.; Durkut, M.; Hadley, P.; Ribas, X.; Rovira C. *J. Am. Chem. Soc.* **2004**, *126*, 984.

(85) Bromley, S. T.; Mas-Torrent, M.; Hadley, P.; Rovira, C. *J. Am. Chem. Soc.* **2004**, *126*, 6544.

CR030663+